

Rigid Body Rotation in 3-D Space from Body Fixed Acceleration Measurements*

Paul C. Begeman

Padgaonkar et al (1) developed a method for the computation of angular acceleration with respect to the body-fixed (moving) frame using 9 accelerometers and based on the following equations:

$$\dot{\omega}_x = (A_{z1} - A_{z0})/2\rho_{y1} - (A_{y3} - A_{y0})/2\rho_{z3} \quad (1)$$

$$\dot{\omega}_y = (A_{x3} - A_{x0})/2\rho_{z3} - (A_{z2} - A_{z0})/2\rho_{x2}$$

$$\dot{\omega}_z = (A_{y2} - A_{y0})/2\rho_{x2} - (A_{x1} - A_{x0})/2\rho_{y1}$$

where the A's are the measured accelerations from linear accelerometers configured in a 3-2-2-2 cluster as shown in Figure 1. Since Equation 1 is purely algebraic at each time step, the computation is stable and relatively insensitive to small errors in measurement. Computation of angular displacement is difficult due to non-commutativity of finite three-dimensional rotations. Problems are encountered during numerical integration of the transformation matrix,

$$\dot{\underline{D}}_B = \underline{D}_B \cdot [\underline{\omega x}] \quad (2)$$

where

$$[\underline{\omega x}] = \begin{bmatrix} 0 & -\omega_z & \omega_y \\ \omega_z & 0 & -\omega_x \\ -\omega_y & \omega_x & 0 \end{bmatrix}$$

and \underline{D}_B is the transformation matrix of a vector from body-fixed components to inertially-fixed components.

Computation of Euler angles at each time step by the integration of Euler rates can result in singularities (gimbal lock), and a non-orthogonal transformation matrix, especially as errors in ϕ , θ , and ψ accumulate. Similar

*This material is based on a Ph.D. thesis by Naveen K. Mital: "Computation of Rigid Body Rotation in Three-Dimensional Space from Body-Fixed Acceleration Measurements". An abstract of this thesis will appear as a paper in the J. of Applied Mechanics, ASME under the authorship of N. K. Mital and A. I. King.

problems of error accumulation occur when using yaw, pitch and roll. There are two ways of minimizing errors due to non-commutativity. First, the transformation matrix integrated from Equation 2 should be checked for orthogonality and normalized if necessary, and updated at each time step. This method is bound to result in an accumulation of errors as the integration proceeds if the body motion is largely three-dimensional. The second method is to reduce the frequency of updating of the transformation matrix by employing a more sophisticated algorithm as described below.

Bortz (2) presented a new concept in strapdown inertial navigation. A differential equation was derived for the orientation vector relating the body-fixed frame to an inertially-fixed reference frame. The time derivative of this vector is the sum of an inertially measurable angular velocity vector ($\underline{\omega}_B$) and of an inertially non-measurable non-commutative rate vector ($\dot{\underline{\sigma}}_B$). It is precisely this non-commutative rate vector that causes computational problems during numerical integration of the transformation matrix. The orientation vector formulation allows the non-commutative contribution to be isolated and therefore treated separately and advantageously. This significantly reduces the frequency of the updating of the transformation matrix and the accumulated errors. A vector differential equation for the orientation vector is given by:

$$\dot{\underline{\phi}}_B(t) = \underline{\omega}_B(t) + \dot{\underline{\sigma}}_B(t) \quad (3)$$

$\dot{\underline{\phi}}_B(t)$ is an orientation vector such that, at time t , if the chosen reference frame were rotated about an axis pointing in the direction of $\underline{\phi}_B(t)$ through an angle equal in magnitude to $|\underline{\phi}_B(t)|$, it would be brought into coincidence with the body-fixed frame. $\underline{\omega}_B(t)$ is that component of $\dot{\underline{\phi}}_B(t)$ which is due to inertially measurable angular motion, and $\dot{\underline{\sigma}}_B$ is that component of $\dot{\underline{\phi}}_B(t)$ which is due to a non-inertially measurable angular motion.

The transformation matrix D_B can be expressed as a unique matrix function of the rotation vector $\underline{\phi}_B$:

$$\underset{\sim}{D}_B = \frac{1}{\phi_B} \{ \underset{\sim}{\phi}_B \underset{\sim}{\phi}_B^T (1 - \cos \phi_B) + \phi_B^2 \underset{\sim}{I} \cos \phi_B + \phi_B^2 \frac{\sin \phi_B}{\phi_B} [\underset{\sim}{\phi} \times] \}. \quad (4)$$

Using Equations 2, 3 and 4 provides a solution for $\dot{\underset{\sim}{\sigma}}_B(t)$:

$$\dot{\underset{\sim}{\sigma}}_B = \frac{1}{2} \underset{\sim}{\phi}_B \times \underset{\sim}{\omega}_B + \frac{1}{\phi_B} \left[1 - \frac{\phi_B \sin \phi_B}{2(1 - \cos \phi_B)} \right] \underset{\sim}{\phi}_B \times (\underset{\sim}{\phi}_B \times \underset{\sim}{\omega}_B) \quad (5)$$

Equation 5 shows the interaction of the history of previous rotations of $\underset{\sim}{\phi}_B$ with the current angular velocity $\underset{\sim}{\omega}_B$ to produce the rate vector $\dot{\underset{\sim}{\sigma}}_B$ in which the non-commutative effect accumulates. The effect of non-commutativity is to cause a final orientation after a set of rotations that depends not only on the individual rotations that were executed, but also on the order in which they were taken.

It should be noted that as the integration of Equation 3 proceeds, error in $\underset{\sim}{\phi}_B(t)$ accumulates, especially if the non-commutativity rate vector $\dot{\underset{\sim}{\sigma}}_B(t)$ is significant. In such cases whenever $|\underset{\sim}{\phi}|$ reaches ϕ_{\max} (where ϕ_{\max} is chosen arbitrarily), $\underset{\sim}{\phi}_B$ is reset to zero, the time of reset is labeled t_0 , and the initial condition matrix $\underset{\sim}{D}_B(t_0)$ is updated to reflect the value of $\underset{\sim}{\phi}_B$ just prior to reset. In the conventional method, updating is performed at each time step, while in the orientation vector technique, matrix $\underset{\sim}{D}_B$ is updated after several time steps, whenever $|\underset{\sim}{\phi}_B|$ reaches ϕ_{\max} . The tendency of the computed transformation matrix to become non-orthogonal is attributable to round-off errors during matrix multiplication. The problem becomes more severe as the frequency of generating a new initial condition matrix increases. Thus a satisfactory algorithm should call for less frequent updating of $\underset{\sim}{D}_B$.

Once a transformation matrix is computed at each time step, it can be used to transform a vector or to characterize a rigid body rotation in terms of physical quantities, such as the orientation vector, quaternions, Euler angles or yaw, pitch and roll angles. Except for the singularities in these representations, the direction cosine matrix corresponding to any of the representations is unique, although the converse is not necessarily true.

The method was first tested against hypothetical data involving a sequence of known rigid body rotations. Figure 2 shows a sequence of 90 - degree rotations along the body-fixed x-, y-, and z- axes. The hypothetical components of ω_B in the shape of a half-sine wave of duration 50 ms are shown in Figure 3. The amplitude of the components of ω_B were computed so that it rotated the body exactly 90 degrees in 50 ms. Figure 4 shows the orientation vector magnitude and Figure 5 the direction of the effective axis of rotation. Figure 6 shows the quaternions and Figure 7 the yaw, pitch, and roll angles which were corrected for singularity as pitch went through 90 degrees of rotation. Figures 4-7 indicate that the computation of rotations were exact and no instability was observed. The order of rotations was changed to check for the sensitivity of the computation of rotation to the order of rotation. Again the computed rotations were exact and took into account the order of rotation.

Then, rigid body rotations computed from 9 linear accelerometer data acquired during impact acceleration tests were compared against those obtained from three-dimensional analysis of a Sierra 1050 dummy in a 3-point restraint in an 18-g crash simulation. Figure 8 shows the angular accelerations, $\dot{\omega}_B$, and Figure 9 the angular velocities, ω . It is evident from Figure 9 that all components of ω_B are significantly large resulting in large three-dimensional rotations of the head. The computed orientation vector magnitude and its directions are shown in Figures 10 and 11 respectively along with their comparison to film analysis. Figures 12 and 13 show the yaw, pitch and roll and quaternions respectively and film comparisons. The latter correlated well with computed results, thus confirming the method.

Results of another dummy run, without a shoulder belt, so that there was large torso motion, are shown in Figures 14-18. Again the comparisons with film analysis show excellent agreement. For this case computation of yaw, pitch, and roll angles caused problems (Figure 18) as pitch went through 90 degrees.

To study the sensitivity of rotational computations to an error in ω_B , three specific cases were implemented:

Case 1: $\omega_x = 4$ rad/s peak-to-peak at 30 Hz

$\omega_y = 40$ rad/s peak-to-peak at 10 Hz

$\omega_z = 0$

Case 2: $\omega_x = 2$ rad/s peak-to-peak at 30 Hz with an offset of 2 rad/s

$\omega_y = 40$ rad/s peak-to-peak at 10 Hz

$\omega_z = 0$

Case 3: $\omega_x = 4$ rad/s peak-to-peak at 30 Hz with an offset of 4 rad/s

$\omega_y = 40$ rad/s peak-to-peak at 10 Hz

$\omega_z = 0$

Figure 19 shows the ω_B components for Case 1. The y - axis was the major axis of rotation and ω_x was an error component (10%). Figures 20 and 21 show the orientation vector and direction, Figure 22 yaw, pitch and roll, and Figure 23 the quaternions. It is evident that the 10% sinusoidal error with no offset has not caused errors in rotation computation.

Figure 24 shows the ω_B components for Case 2, 5% sinusoidal error plus 5% offset error. Figures 25-28 show the three-dimensional rotation. Build up of errors is evident in yaw, pitch, and roll at 200 ms.

Figure 29 shows the ω_B components for Case 3, 10% sinusoidal error plus 10% offset. Figures 30-33 show the rotation which deviate significantly from the rotations of Case 1.

It has been shown that the 9 - accelerometer package configured in a 3-2-2-2 cluster can be used to compute accurate 3-D rotations using the orientation vector scheme, even for large rotations and high accelerations. The method is insensitive to sinusoidal errors but small offsets can lead to large rotational errors, particularly if data are required for long time durations (1 second or longer).

References

1. Padgaonkar, A. J., Krieger, K. W., and King, A. I., "Measurement of Angular Acceleration of a Rigid Body Using Linear Accelerometers", Journal of Applied Mechanics, Sept. 1975.
2. Bortz, J. E., "A New Concept in Strapdown Inertial Navigation", NASA Technical Report TR-329, March 1970.

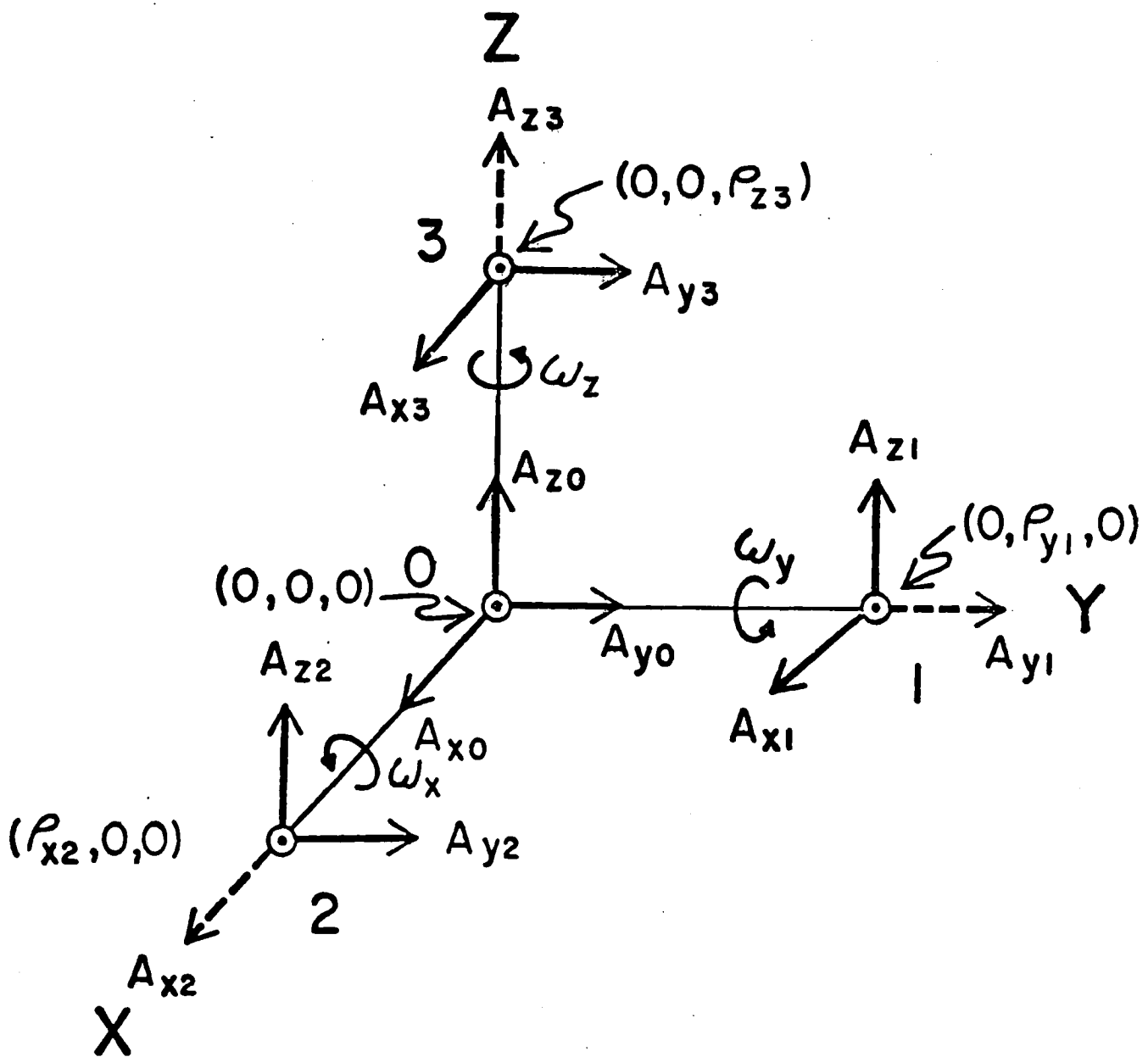


Figure 1
Locations of Accelerometers
on Nine-Accelerometer Module

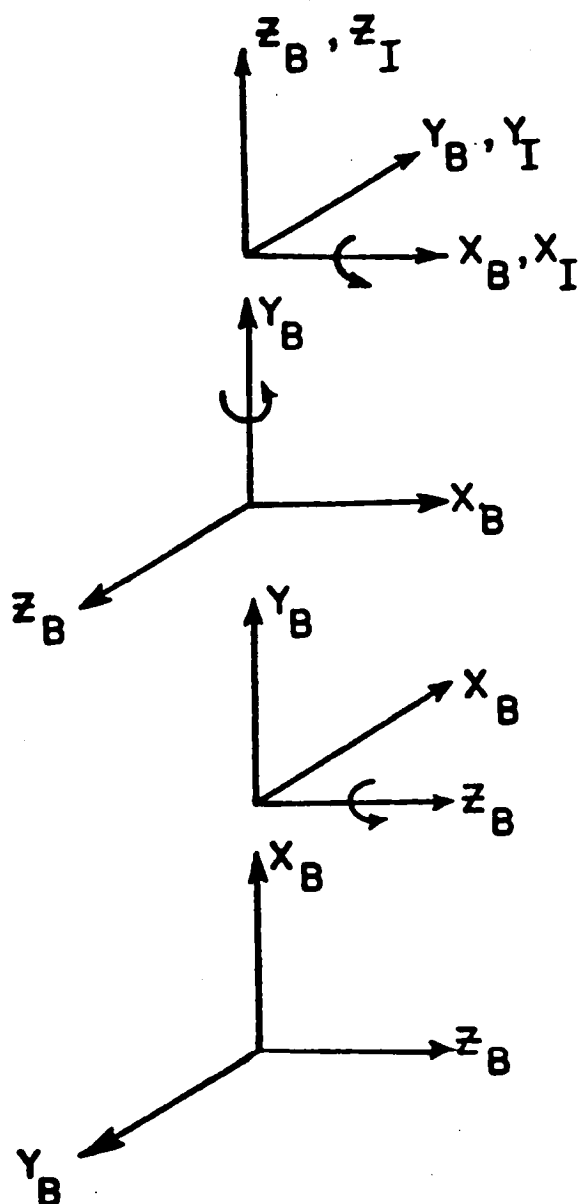
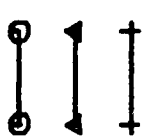


Figure 2
 Sequence of 90-degree Rotations About the Body-fixed
 X-, Y-, and Z- axes

HYP: XYZ-90 SINE



 WX (B)

 WY (B)

 WZ (B)

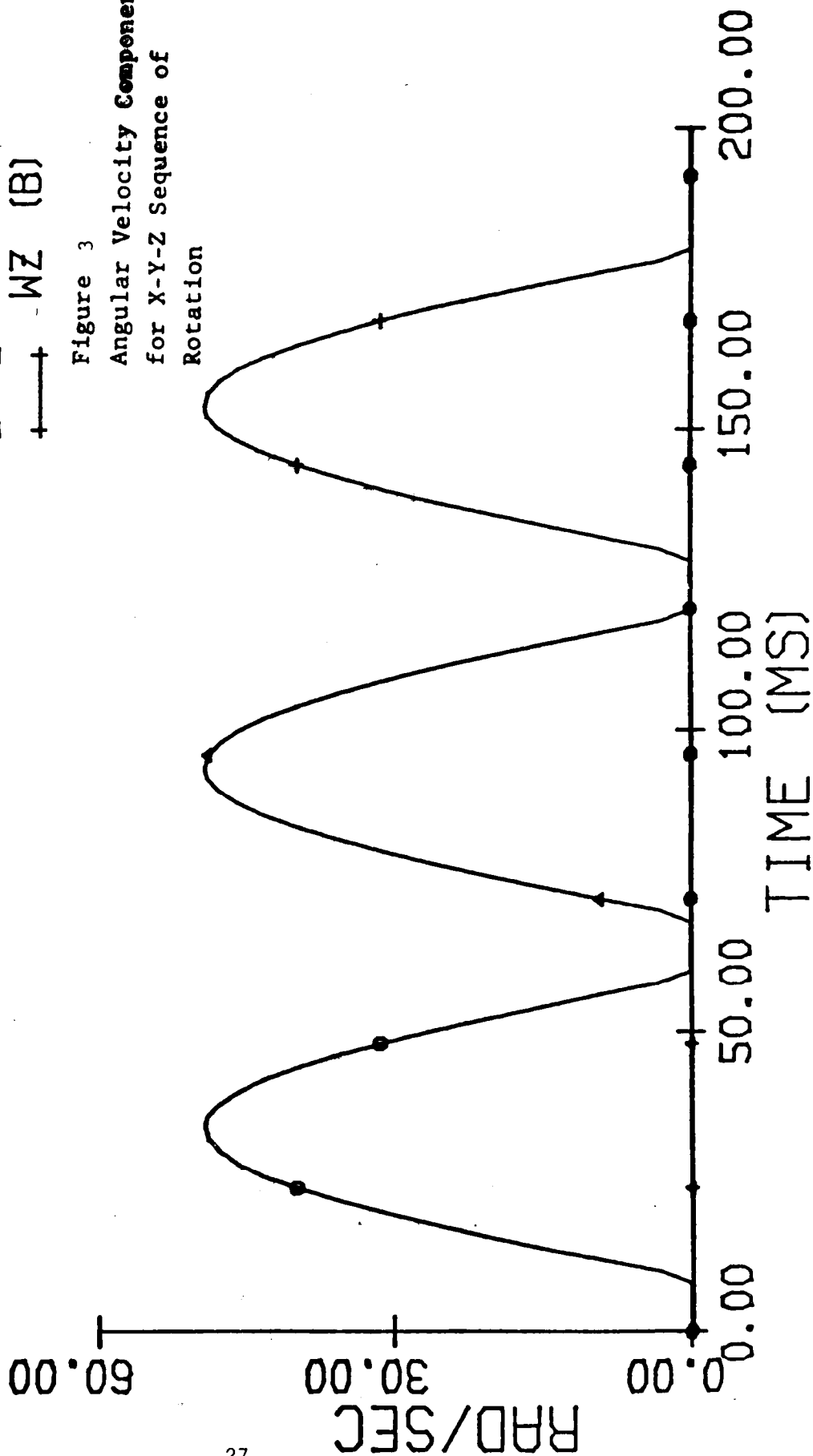


Figure 3
 Angular Velocity Components
 for X-Y-Z Sequence of
 Rotation

HYP: XYZ-90 SINE

THETA

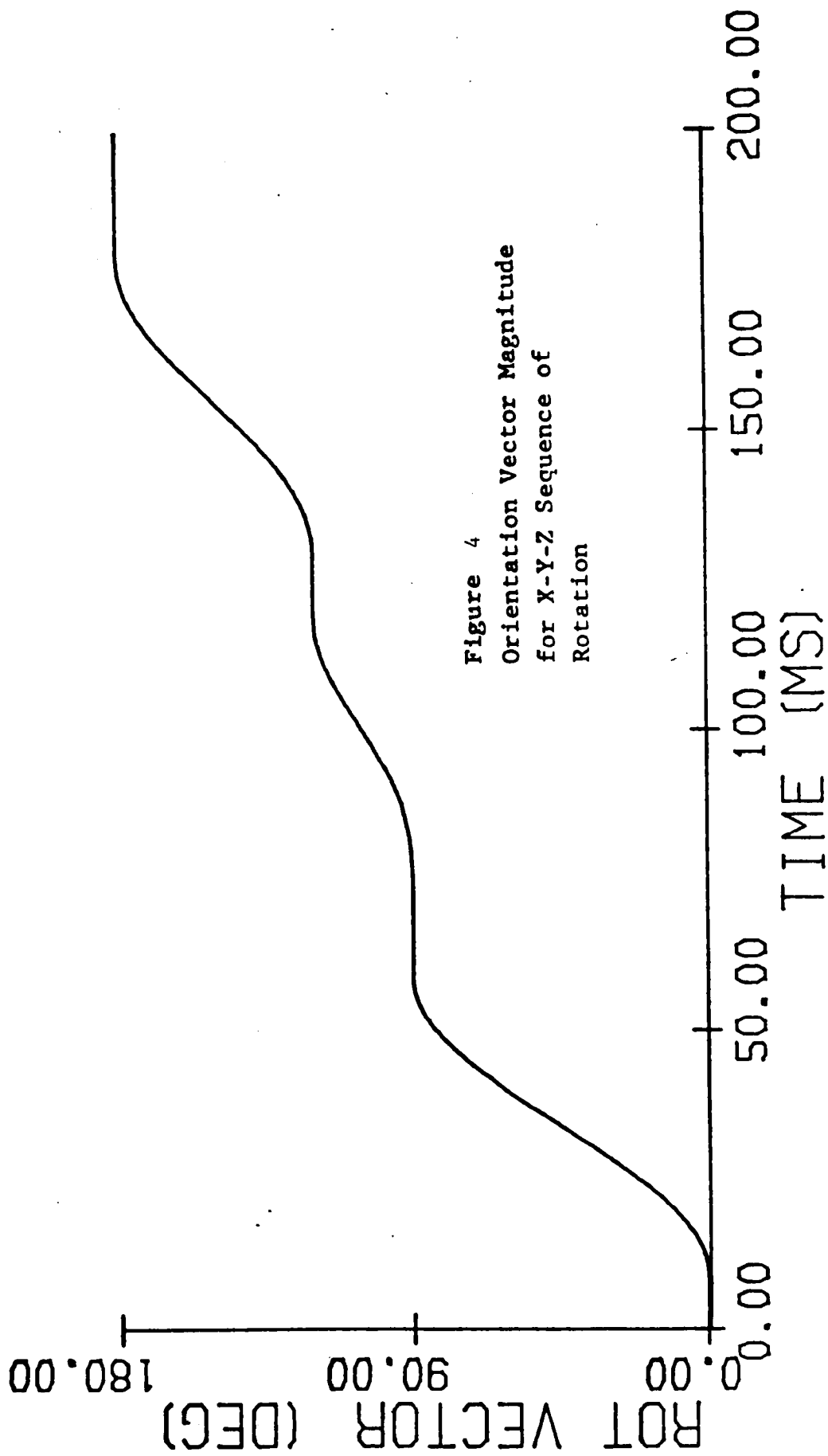


Figure 4
Orientation Vector Magnitude
for X-Y-Z Sequence of
Rotation

HYP: XYZ-90 SINE

TH-I
TH-J
TH-K

○
▲
+

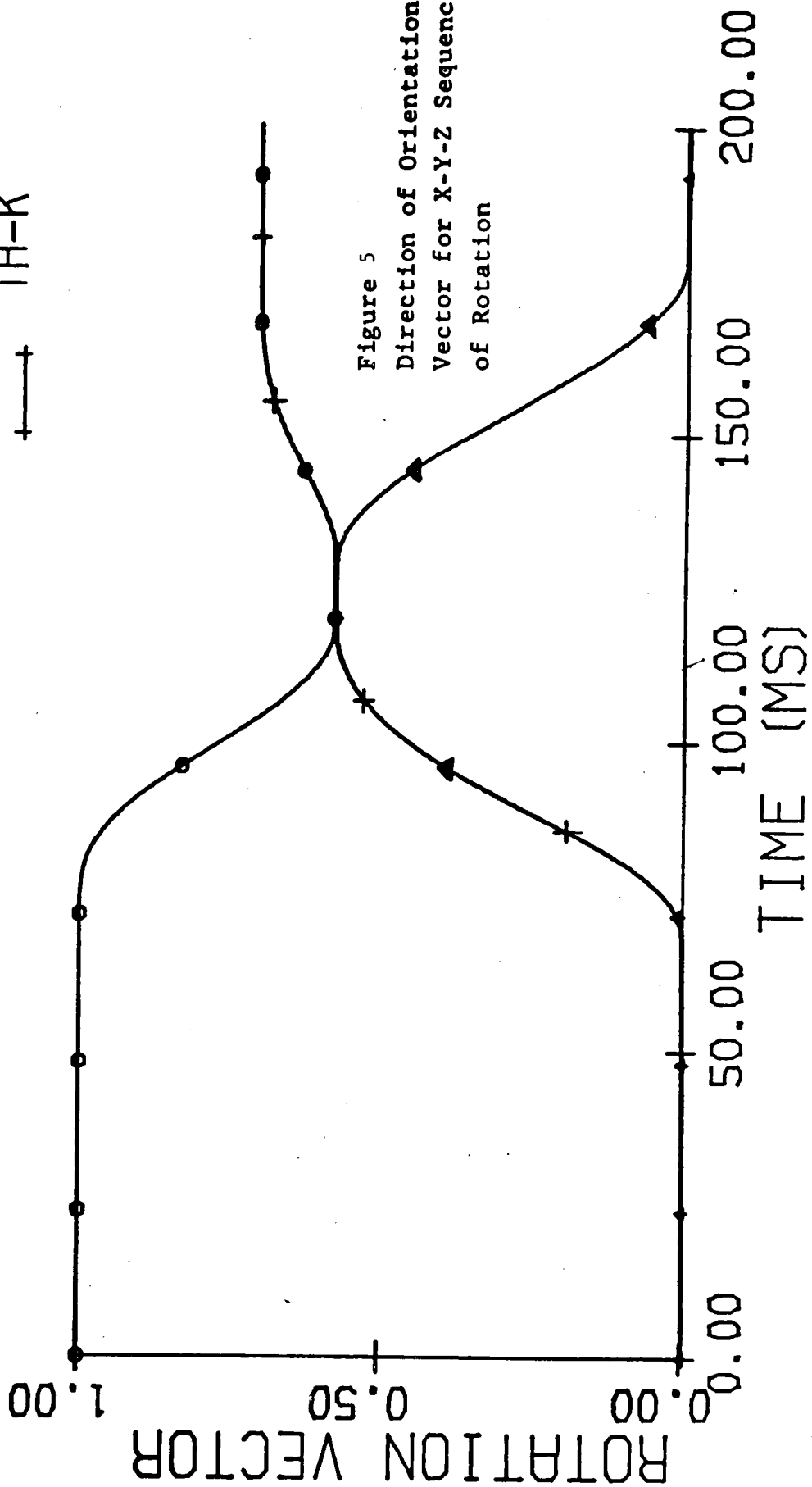
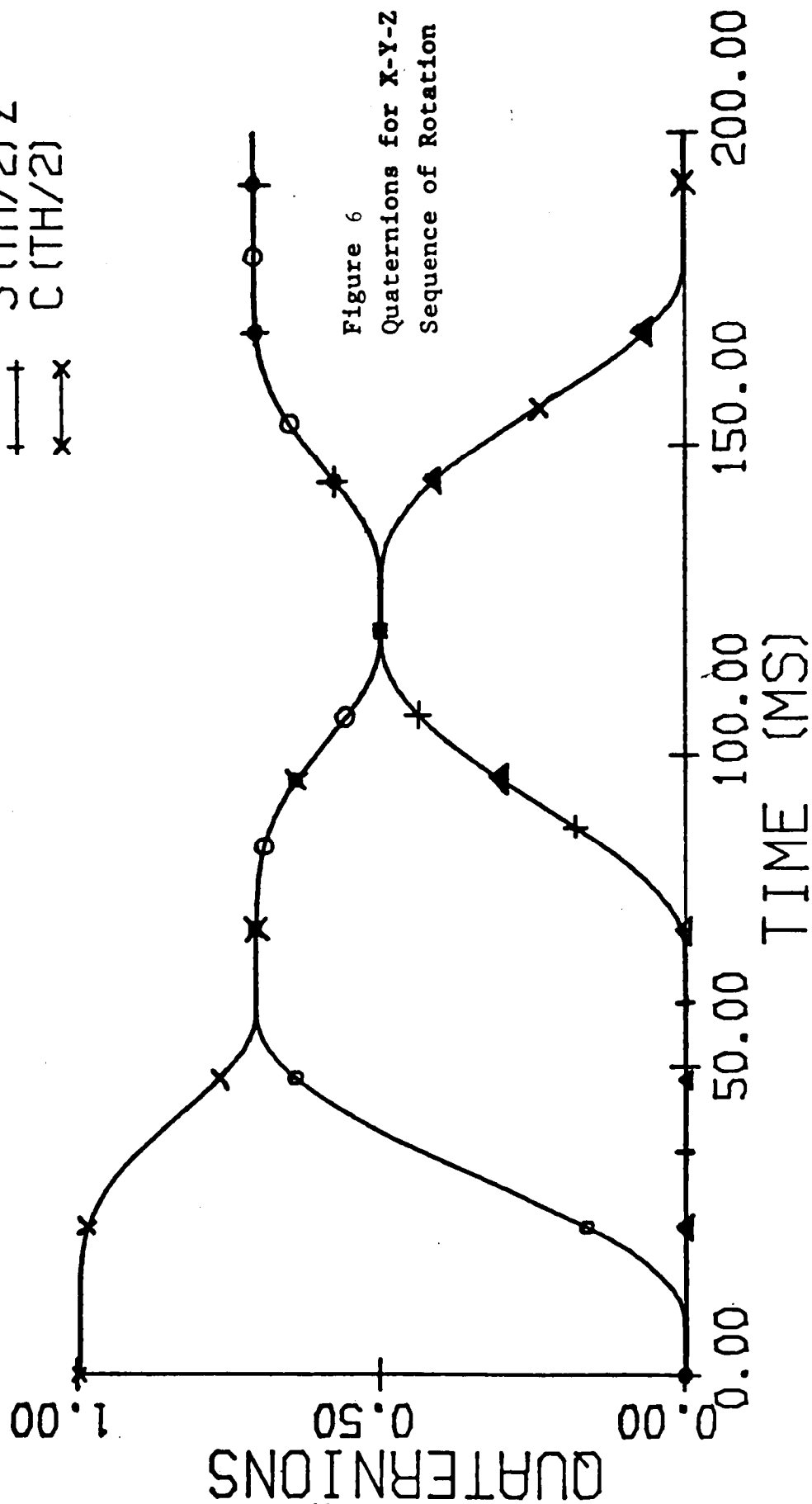


Figure 5
Direction of Orientation
Vector for X-Y-Z Sequence
of Rotation

HYP: XYZ-90 SINE

S (TH/2) X
S (TH/2) Y
S (TH/2) Z
C (TH/2)

○
▲
+
x



HYP: XYZ-90 SINE

YAW
PITCH
ROLL

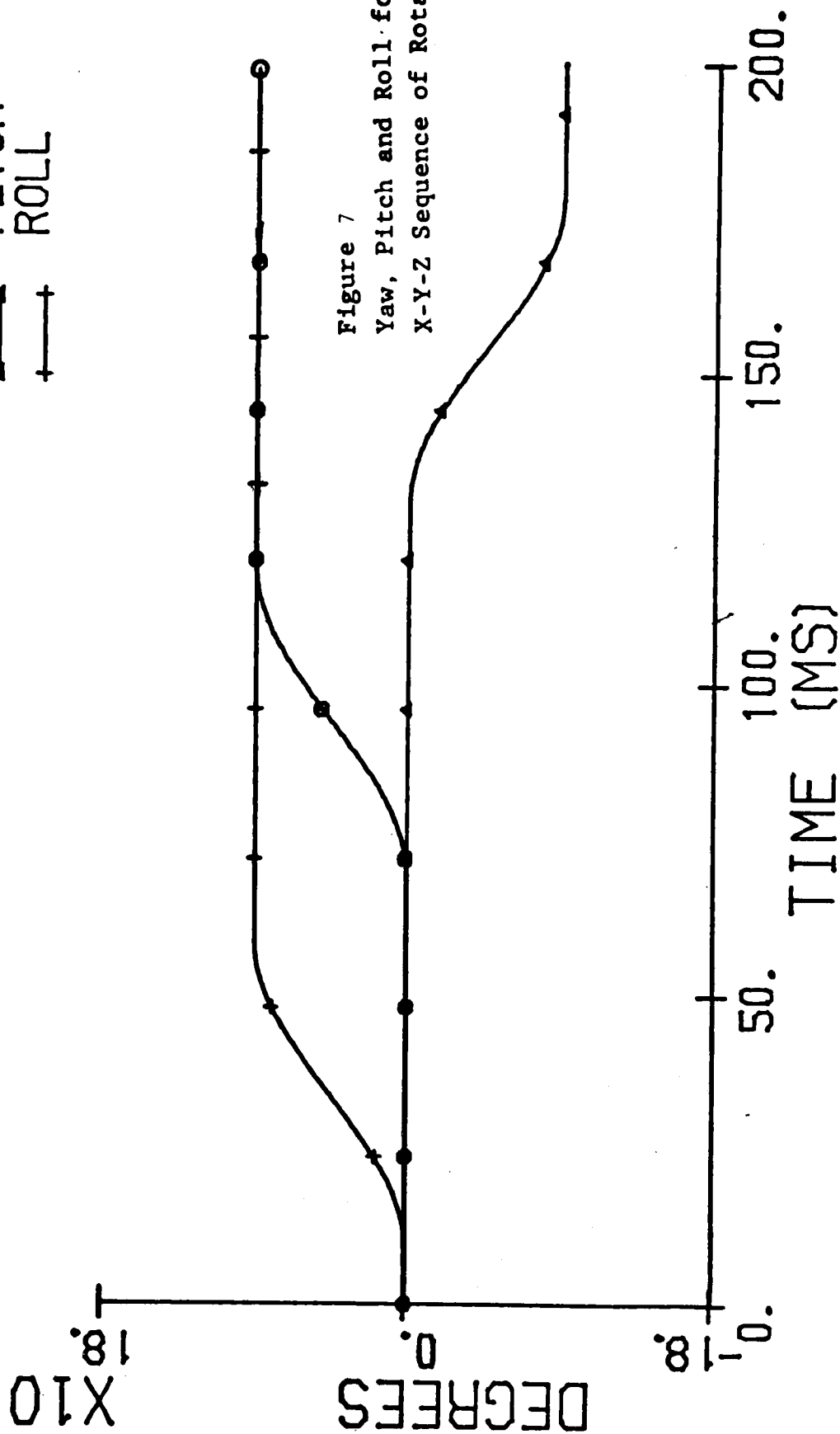


Figure 7
Yaw, Pitch and Roll for
X-Y-Z Sequence of Rotation

DOIV: D367 (1 SHB, 1 G)
 FILTER 100 HZ.

○ DWX (B)
 ▲ DWY (B)
 + DWZ (B)

$\times 10^2$

RAD/SEC/SEC

15.00

0.00

10.00

20.00

30.00

40.00

TIME (MS)

$\times 10$

Figure 8
 Angular Acceleration Components for Run D367

D367: 1 SHB 15G
 FILTER 100 HZ.

○ — WX (B)
 ▲ — WY (B)
 + — WZ (B)

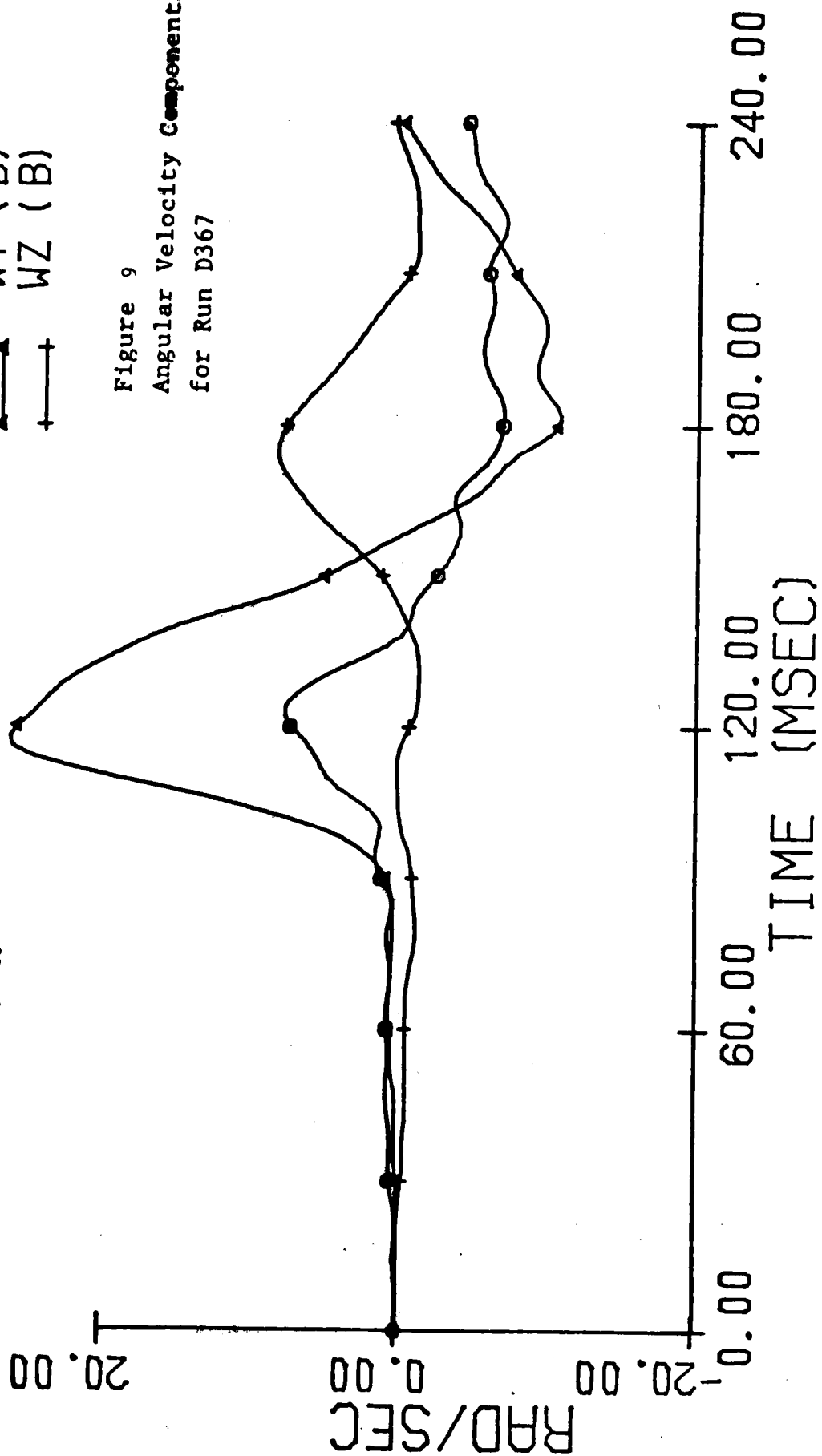


Figure 9
 Angular Velocity Components
 for Run D367

D367: 1 SHB 15G
FILTER 100 HZ

--- THETA (3D FILM)
— THETA (9 ACCEL
METHOD)

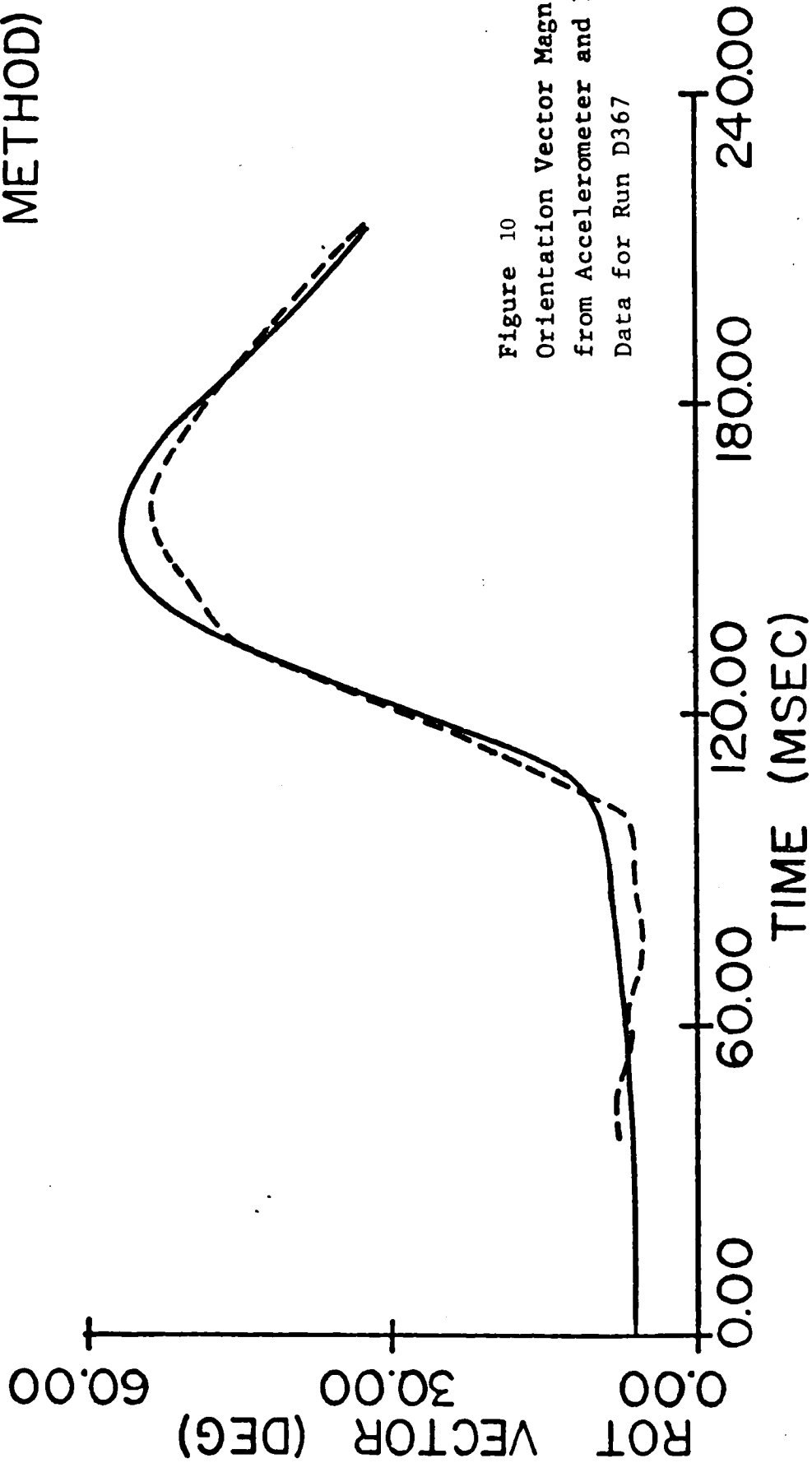


Figure 10
Orientation Vector Magnitude
from Accelerometer and Film
Data for Run D367

D367: 1 SHB 15G
 FILTER 100 HZ.

○---○	} 3D FILM ANALYSES
▲---▲	
+---+	
○---○	} 9 ACCEL METHOD
▲---▲	
+---+	

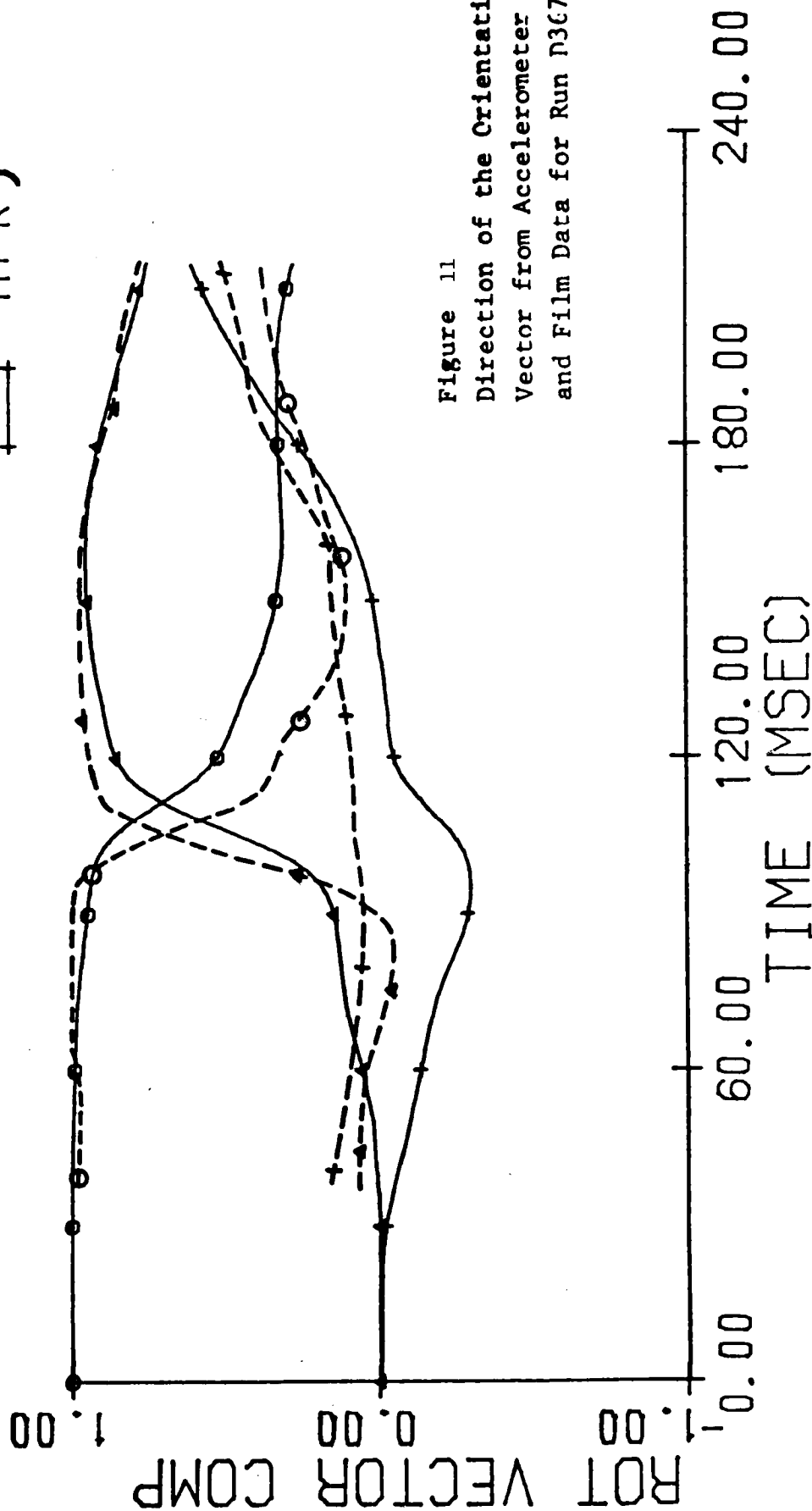


Figure 11
 Direction of the Orientation
 Vector from Accelerometer
 and Film Data for Run D367

D367: 1 SHB 15G
 FILTER 100 HZ.

YAW } 3D FILM
 PITCH } ANALYSES
 ROLL }

YAW } 9 ACCEL
 PITCH } METHOD
 ROLL }

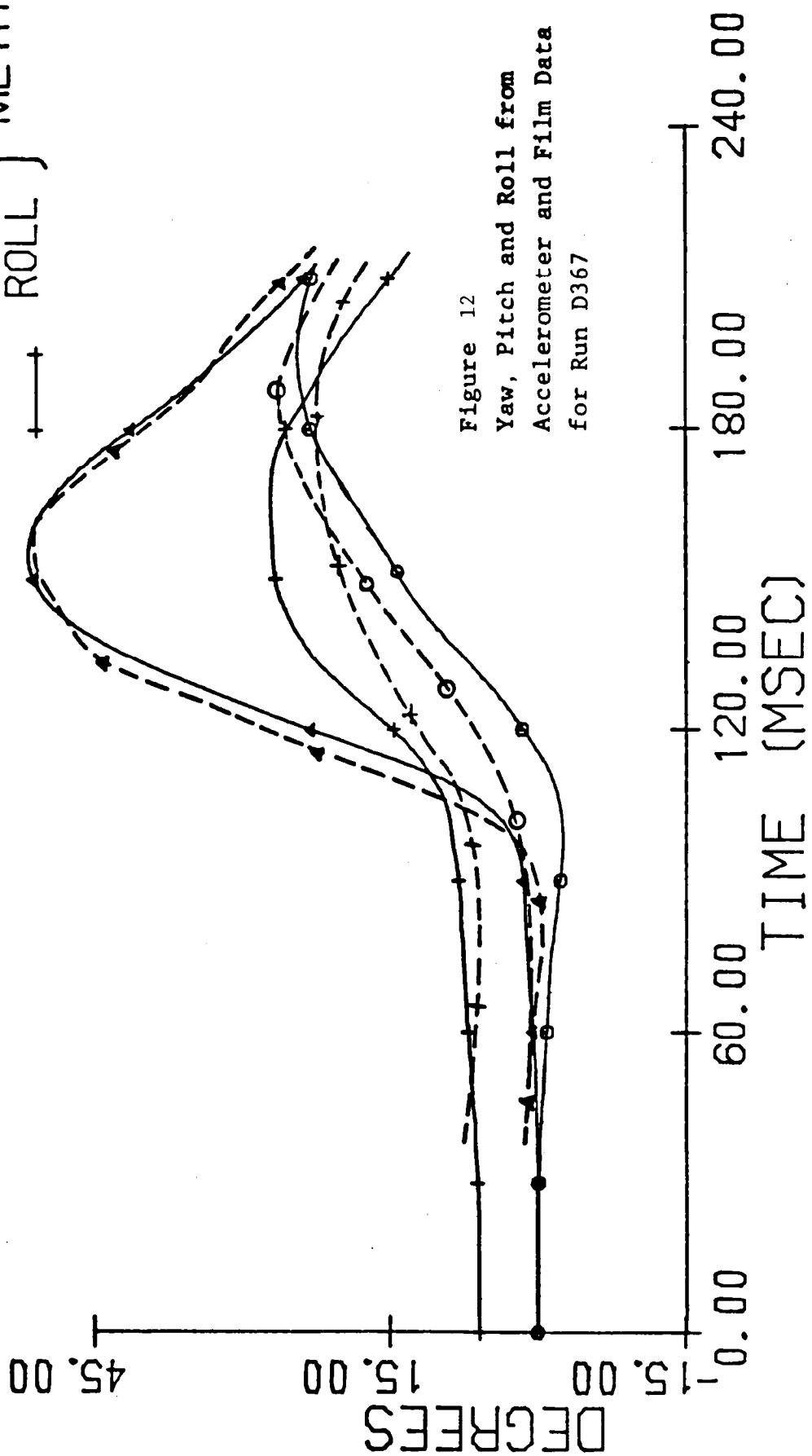


Figure 12
 Yaw, Pitch and Roll from
 Accelerometer and Film Data
 for Run D367

○---○	S(TH/2)X	} 3D FILM
△---△	S(TH/2)Y	
+---+	S(TH/2)Z	
x---x	C(TH/2)	
○---○	S(TH/2)X	} 9
△---△	S(TH/2)Y	
+---+	S(TH/2)Z	
x---x	C(TH/2)	
		ACCEL

D367: 1 SHB 15G
FILTER 100 HZ.

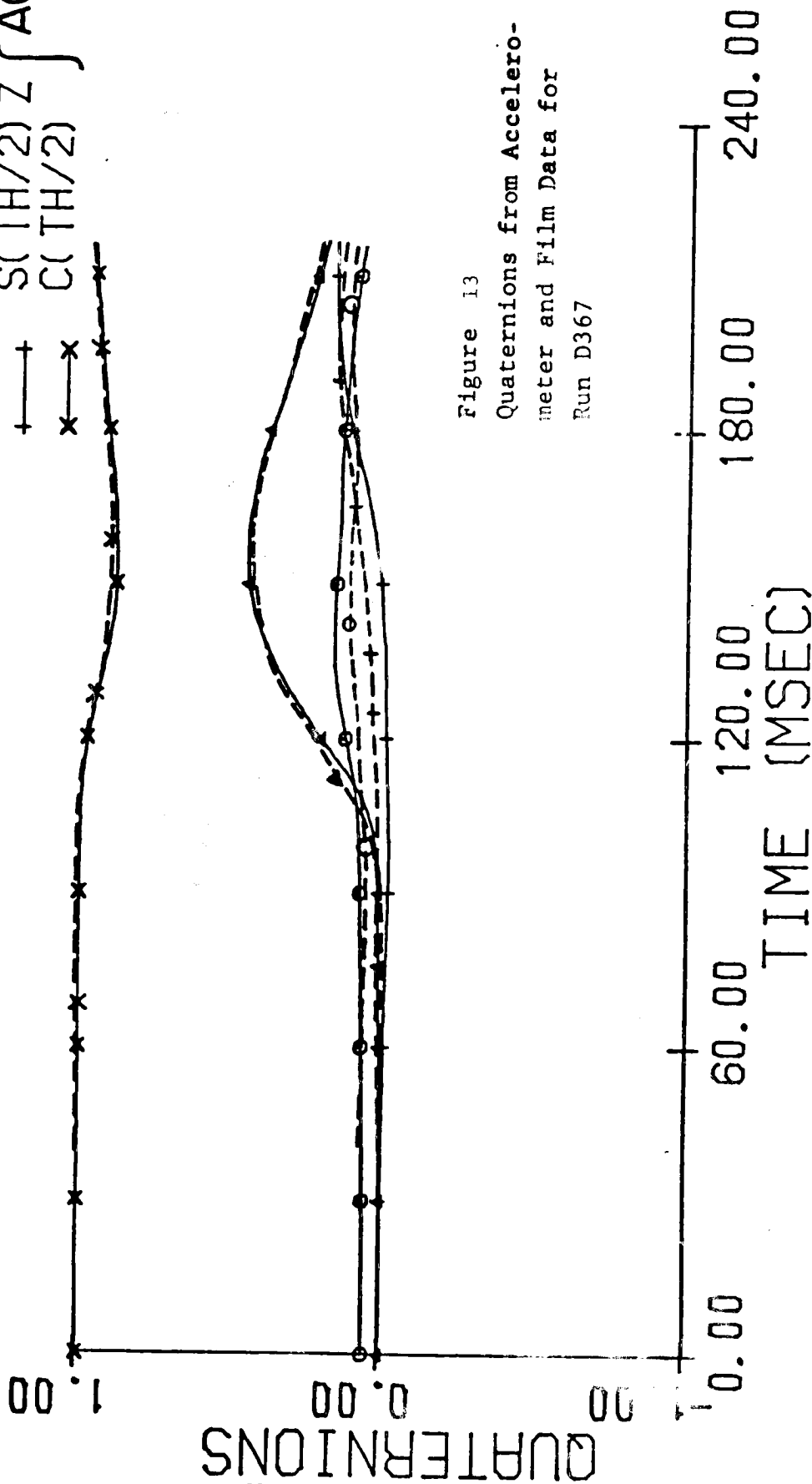


Figure 13
Quaternions from Accelerometer and Film Data for Run D367

D369: NO SHB 18G
 FILTER 100 HZ.

○ — WX (B)
 ▲ — WY (B)
 + — WZ (B)

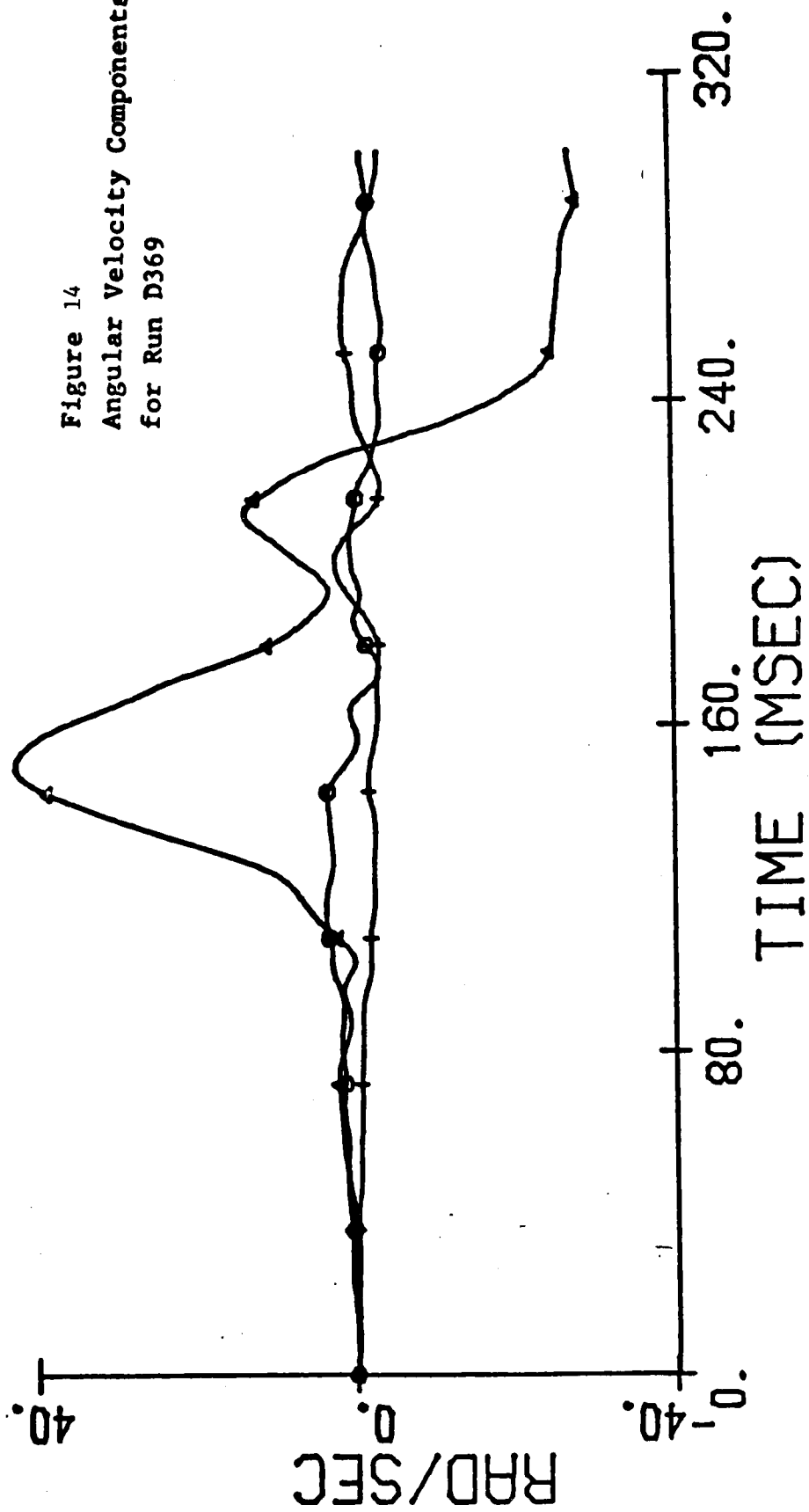


Figure 14
 Angular Velocity Components
 for Run D369

D369: NO SHB 18G
 FILTER 100 HZ.

--- THETA (3D FILM)
 — THETA (9 ACCEL)

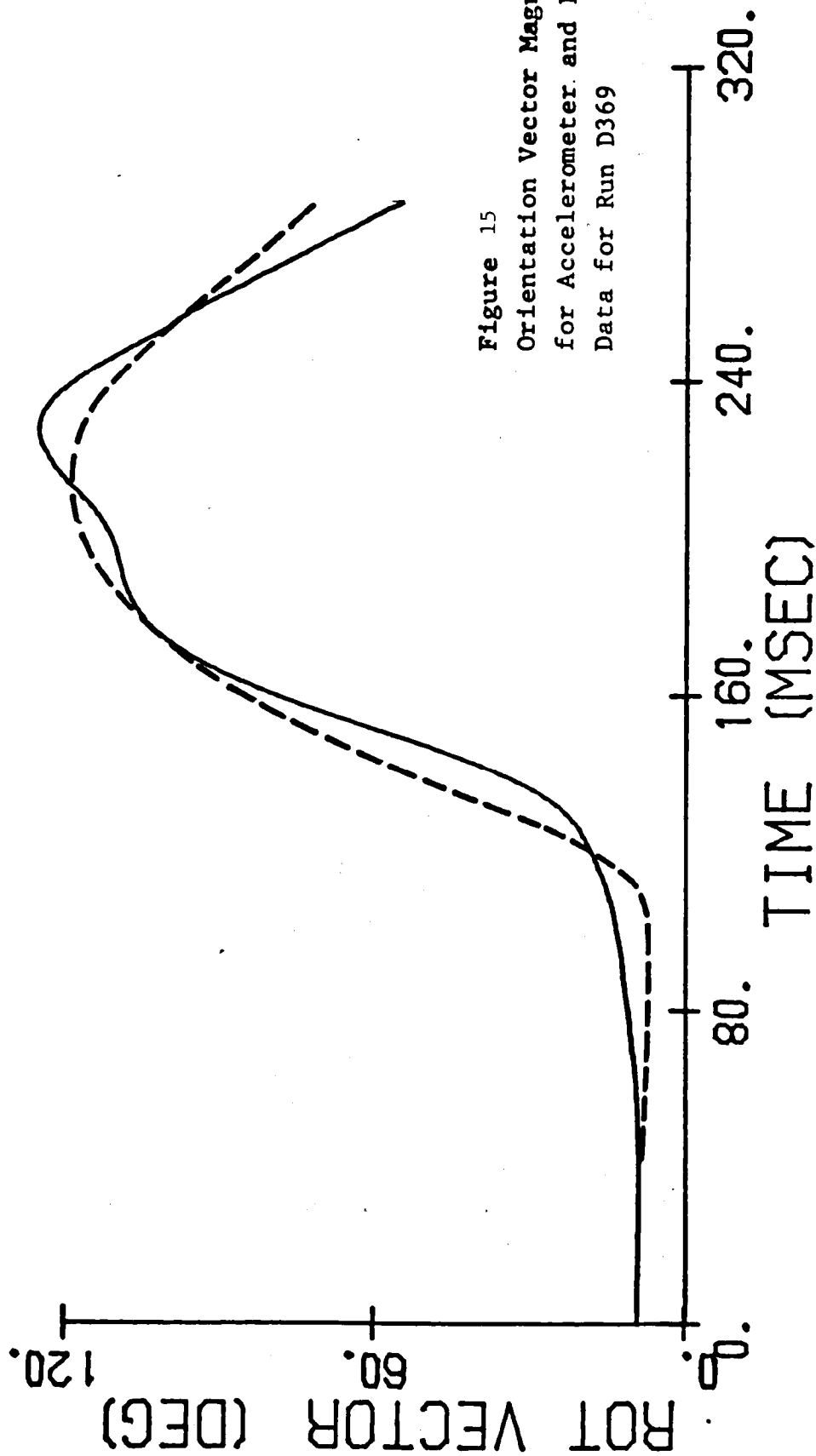


Figure 15
 Orientation Vector Magnitude
 for Accelerometer and Film
 Data for Run D369

TH-I	3D FILM
TH-J	
TH-K	
TH-I	9 ACCEL
TH-J	
TH-K	

D369: NO SHB 18G
 FILTER 100 HZ.

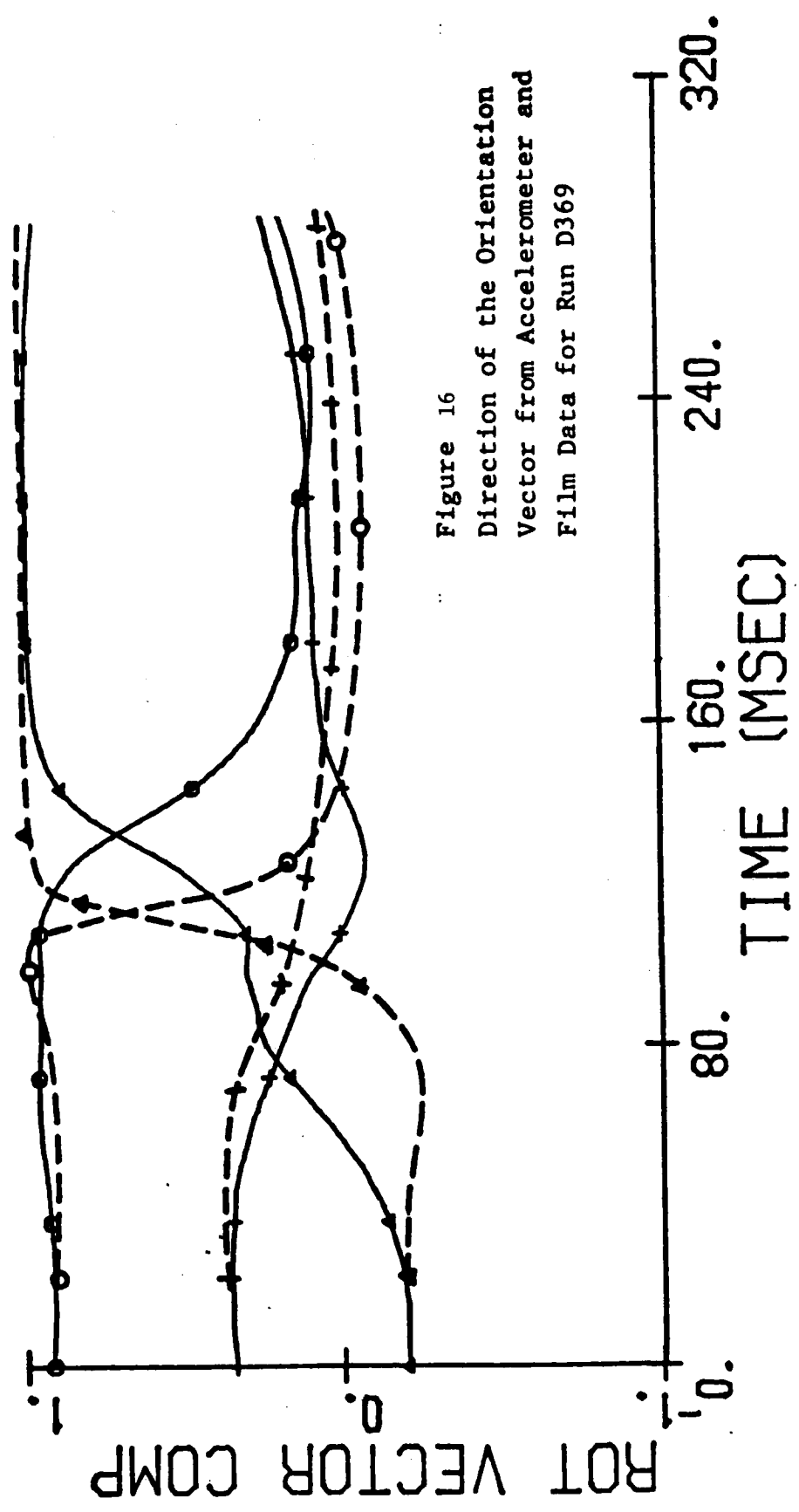


Figure 16
 Direction of the Orientation
 Vector from Accelerometer and
 Film Data for Run D369

S(TH/2)X	3D
S(TH/2)Y	FILM
S(TH/2)Z	
C(TH/2)	
S(TH/2)X	9
S(TH/2)Y	ACC
S(TH/2)Z	
C(TH/2)	

D369: NO SHB 18G
 FILTER 100 HZ.

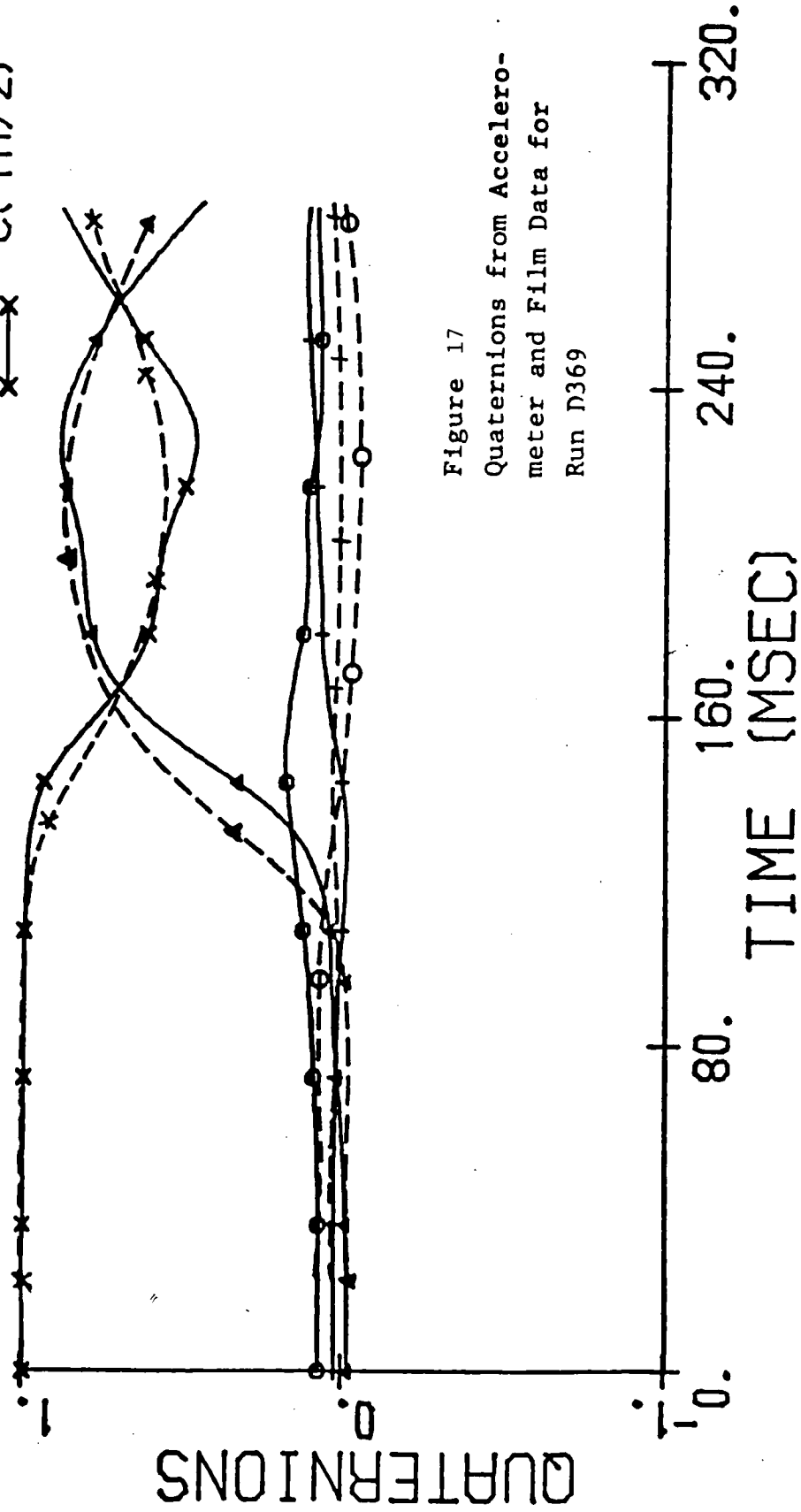


Figure 17
 Quaternions from Accelerometer and Film Data for Run D369

D369: NO SHB 18G
 FILTER 100 HZ.

YAW
 PITCH
 ROLL

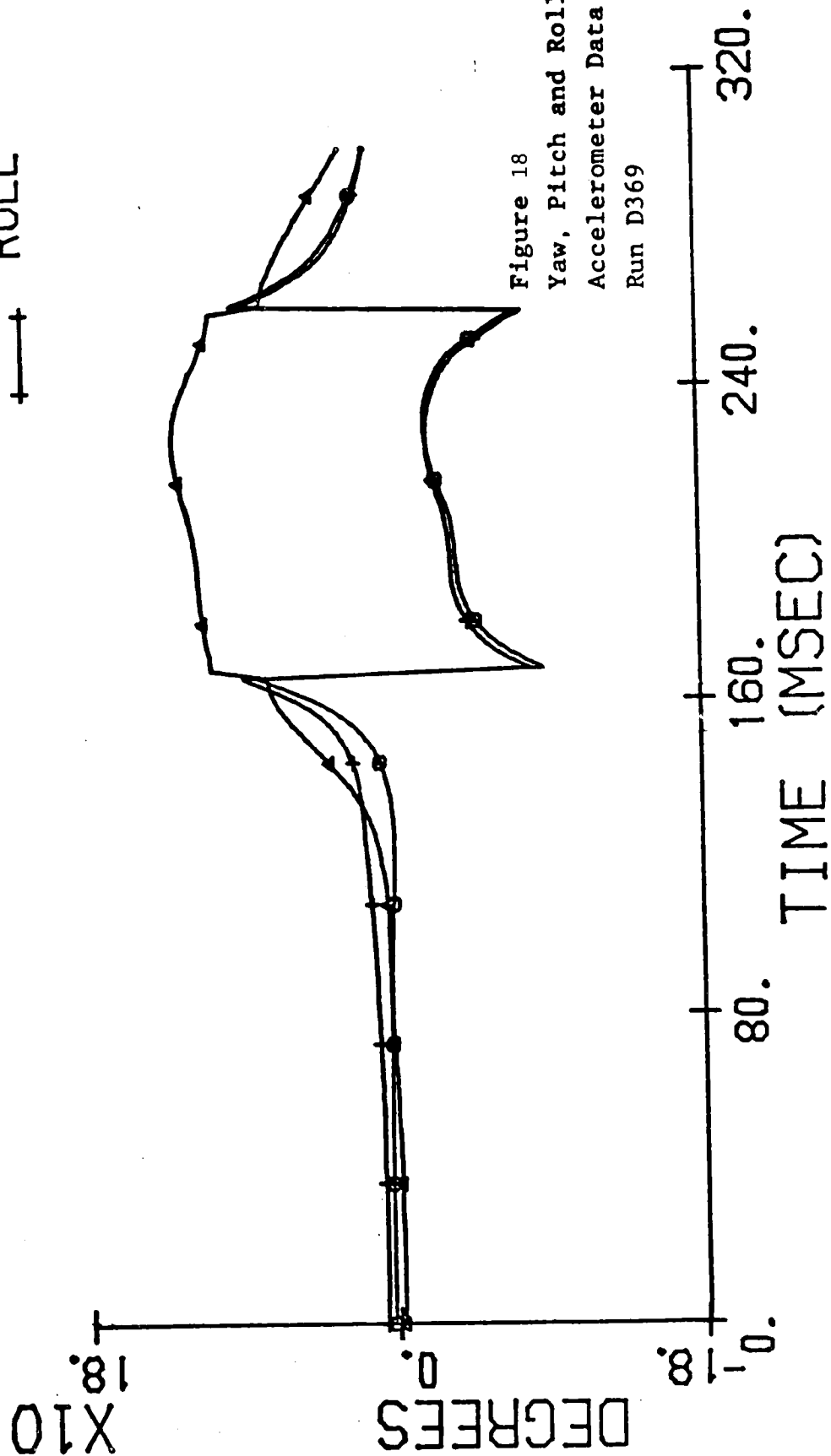


Figure 18
 Yaw, Pitch and Roll from
 Accelerometer Data for
 Run D369

HYPH: CASE 1

○— WX (B)
 ▲— WY (B)
 +— WZ (B)

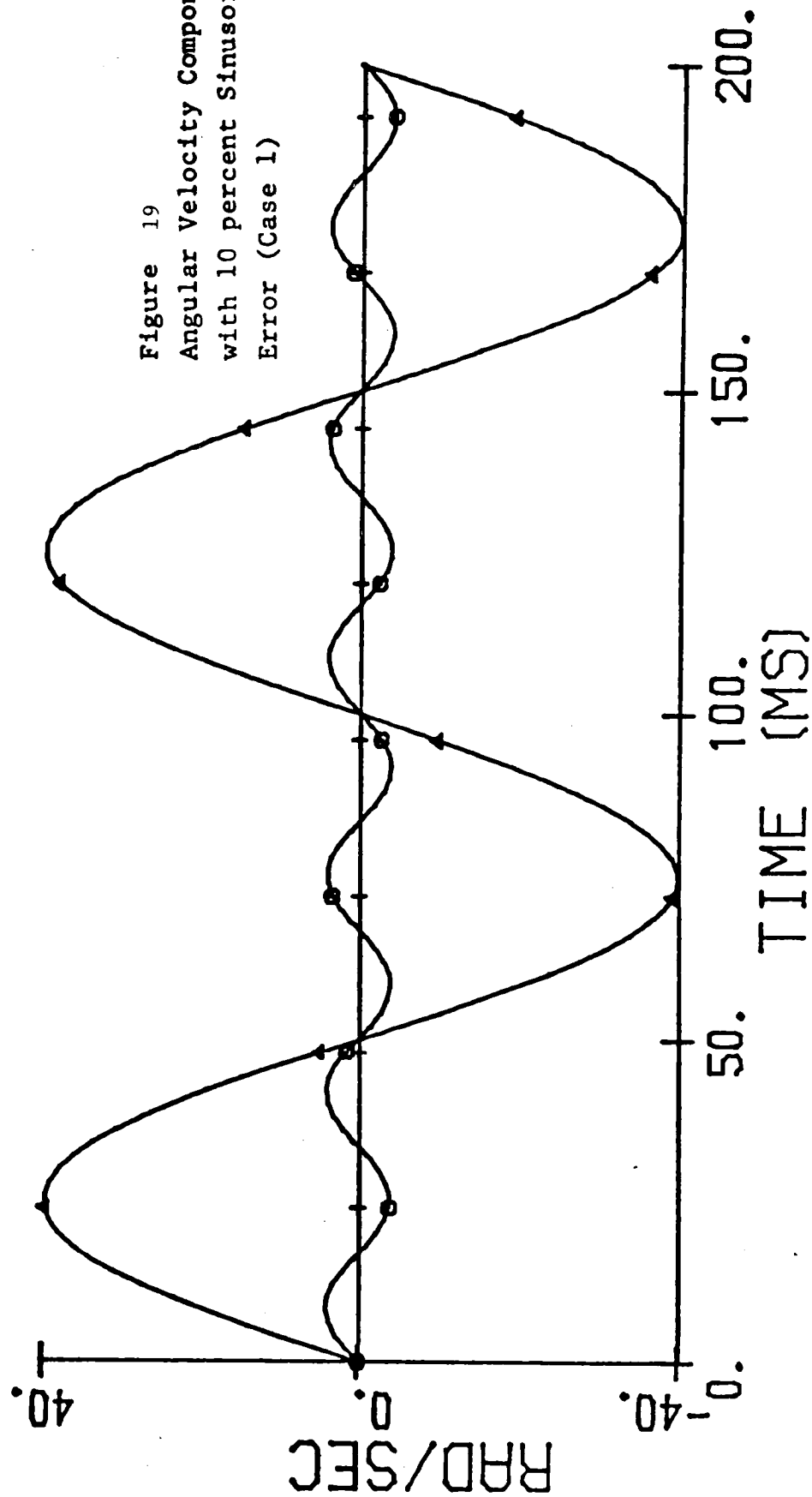
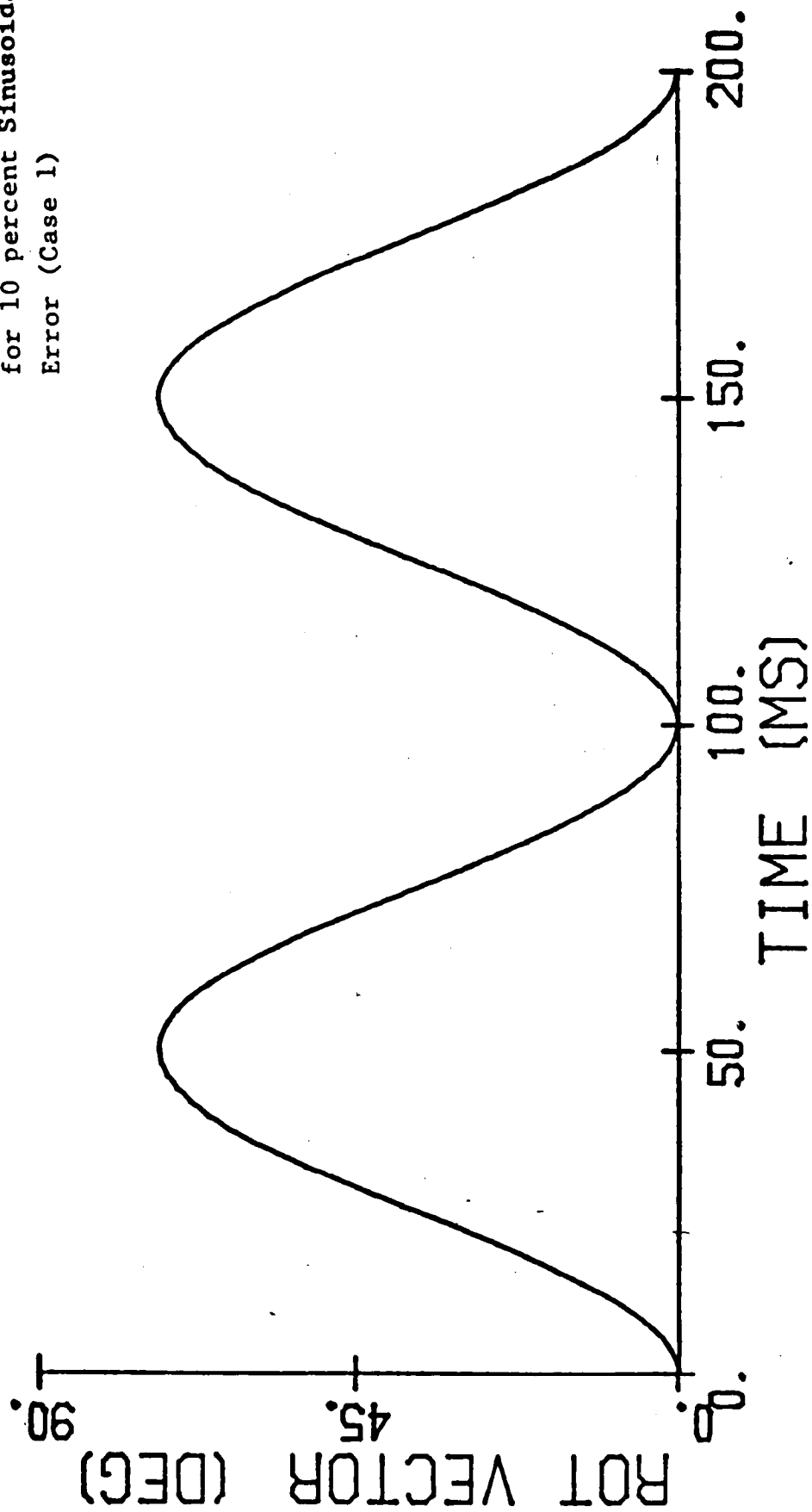


Figure 19
 Angular Velocity Components
 with 10 percent Sinusoidal
 Error (Case 1)

HYPH: CASE 1

THETA

Figure 20
Orientation Vector Magnitude
for 10 percent Sinusoidal
Error (Case 1)



HYPTH: CASE 1

TH-I
TH-J
TH-K

○
△
+

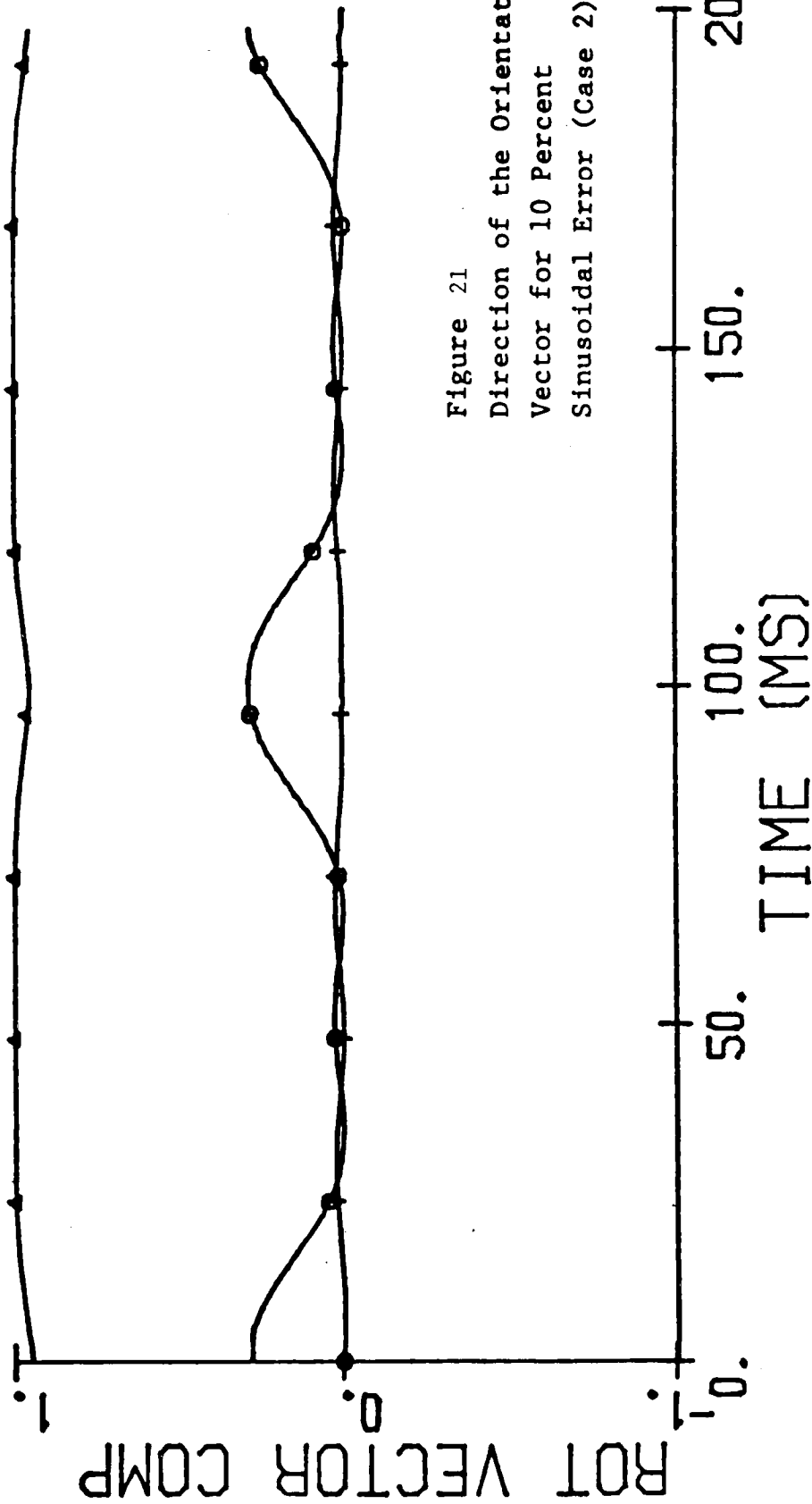
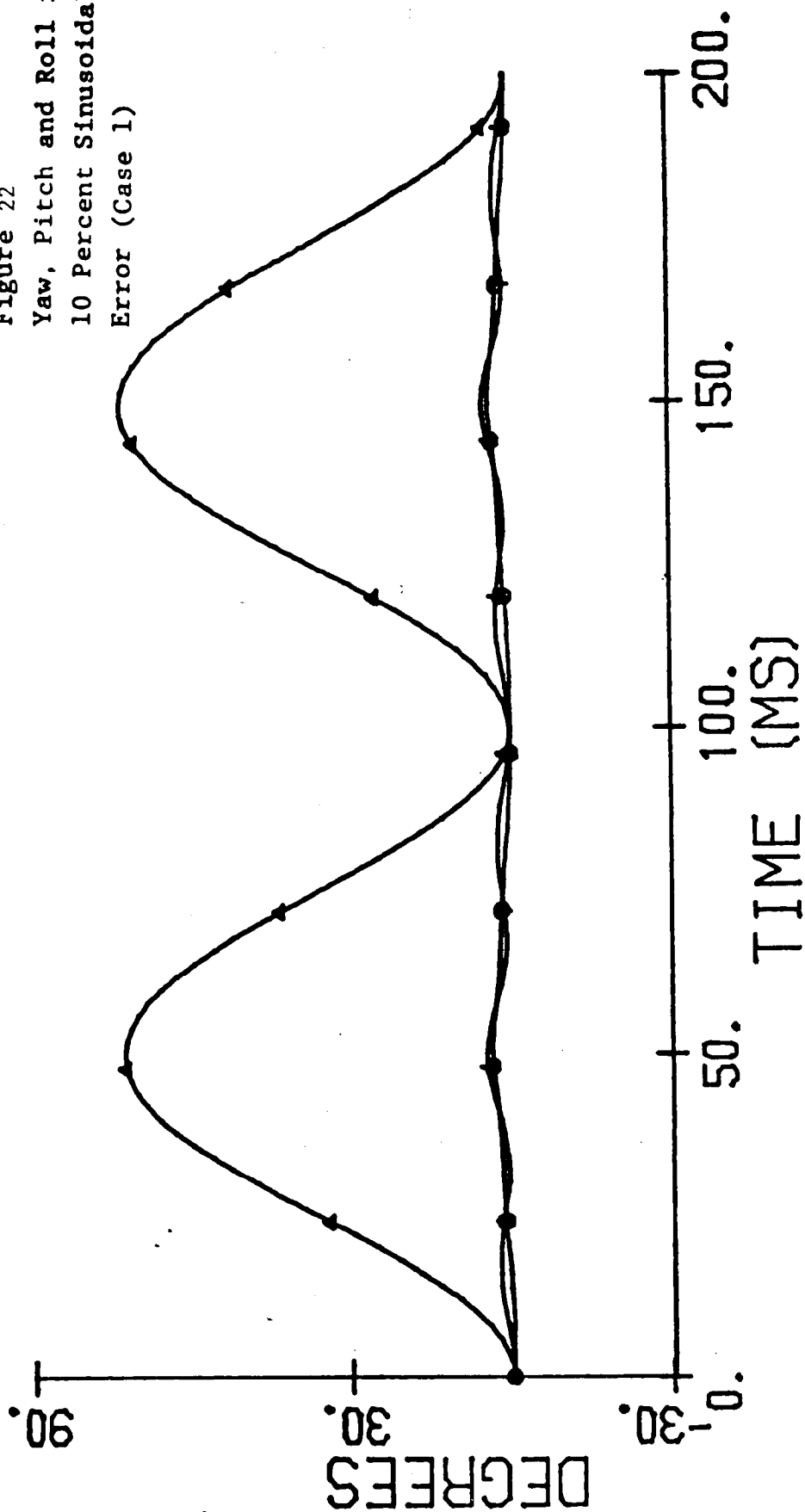


Figure 21
Direction of the Orientation
Vector for 10 Percent
Sinusoidal Error (Case 2)

HYPH: CASE 1

YAW
PITCH
ROLL

Figure 22
Yaw, Pitch and Roll for
10 Percent Sinusoidal
Error (Case 1)



HYPH: CASE 1

S(TH/2) I
S(TH/2) J
S(TH/2) K
C(TH/2)

⊙
▲
+
×

QUATERNIONS

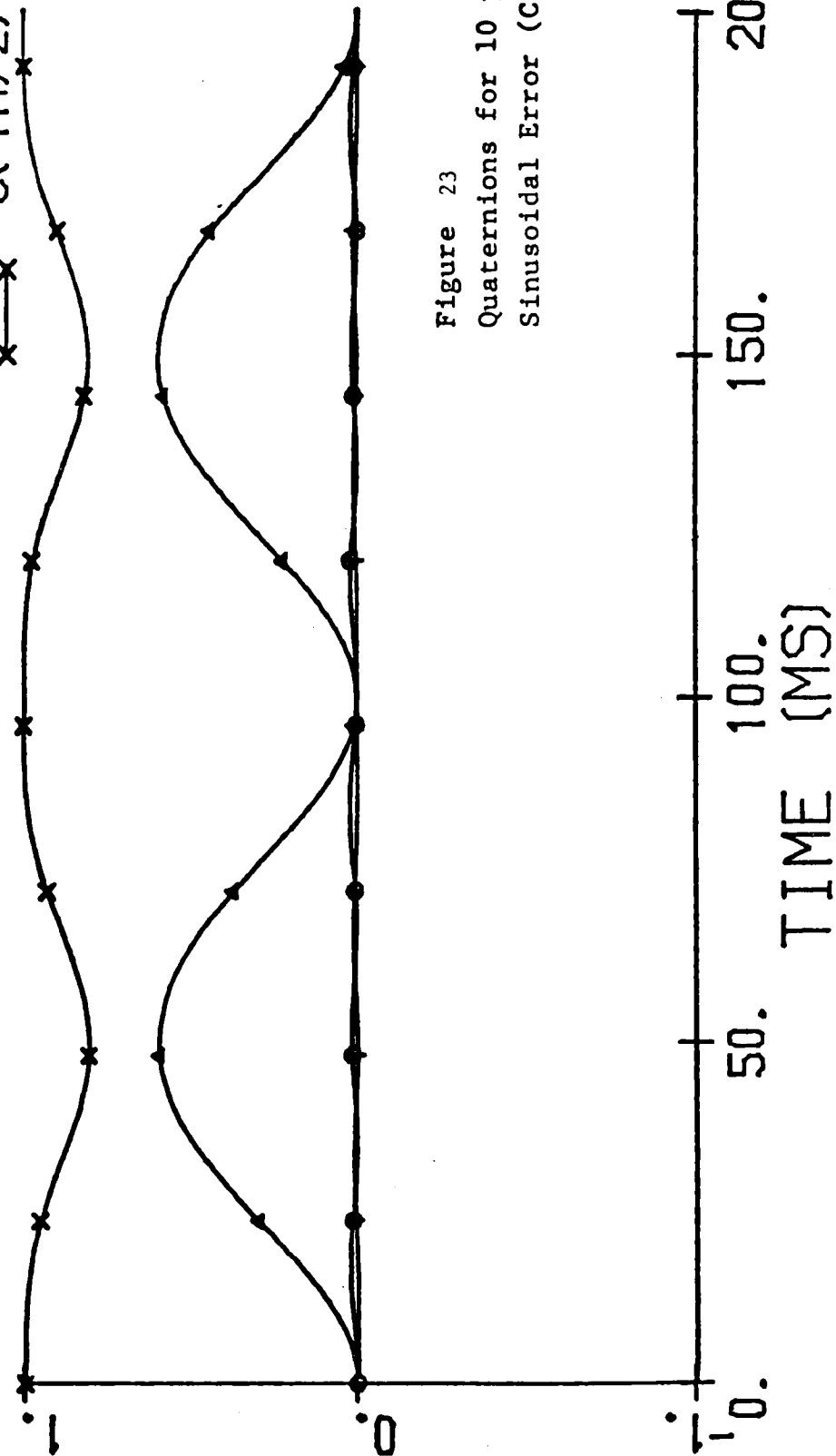


Figure 23
Quaternions for 10 percent
Sinusoidal Error (Case 1)

HYPH: CASE 2

\ominus WX (B)
 \blacktriangle WY (B)
 \dagger WZ (B)

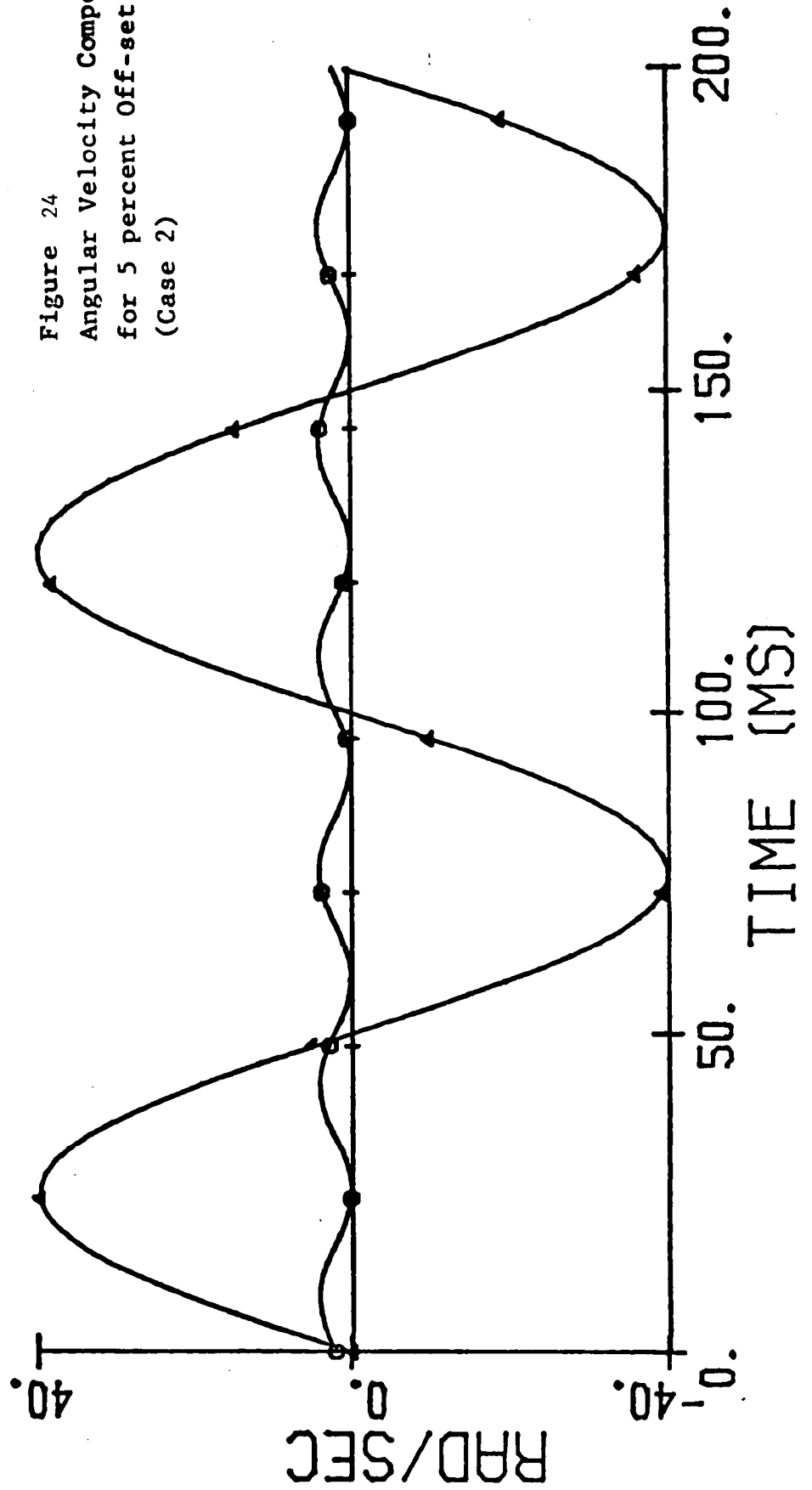
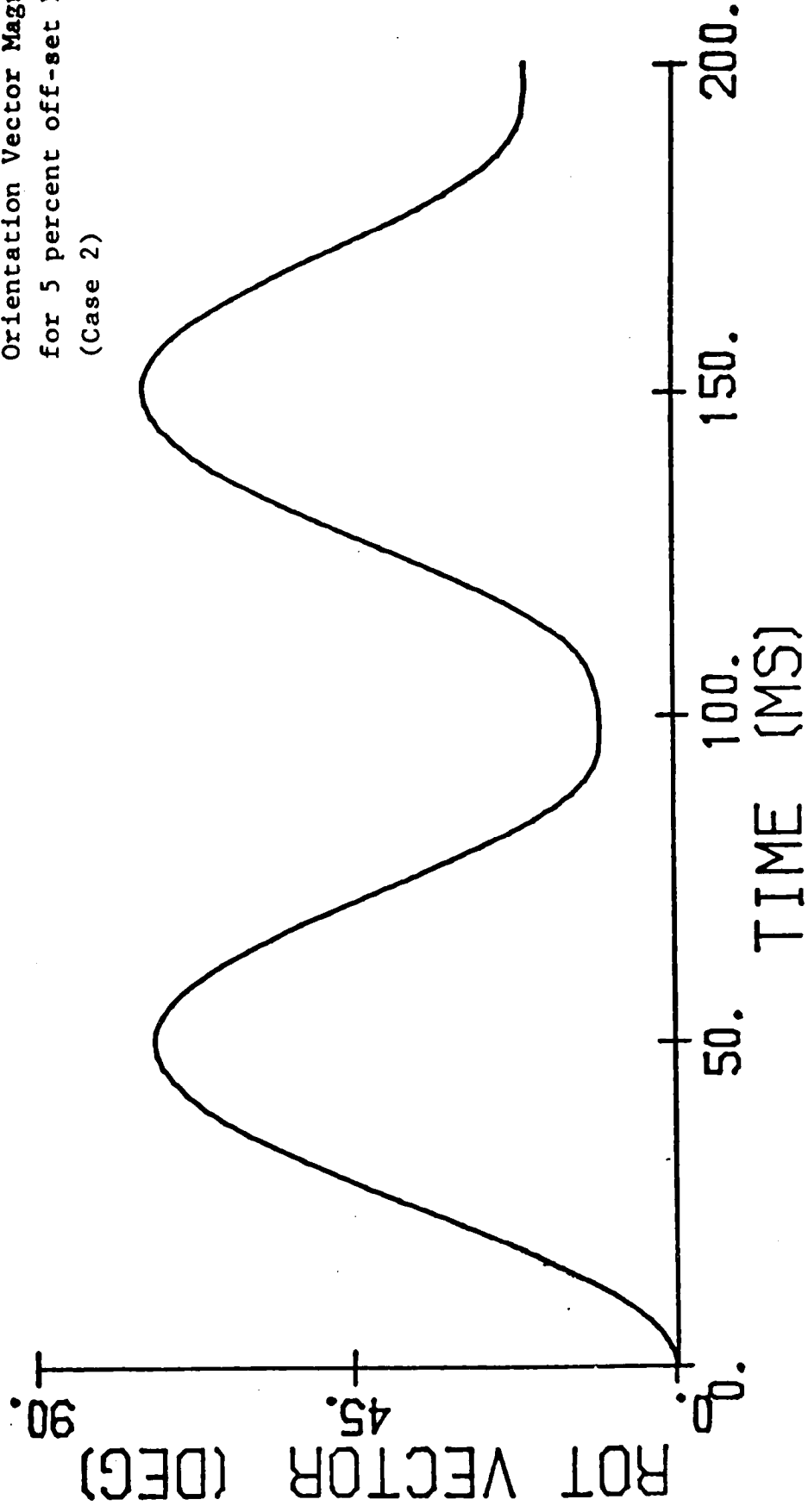


Figure 24
 Angular Velocity Components
 for 5 percent Off-set Error
 (Case 2)

HYPH: CASE 2

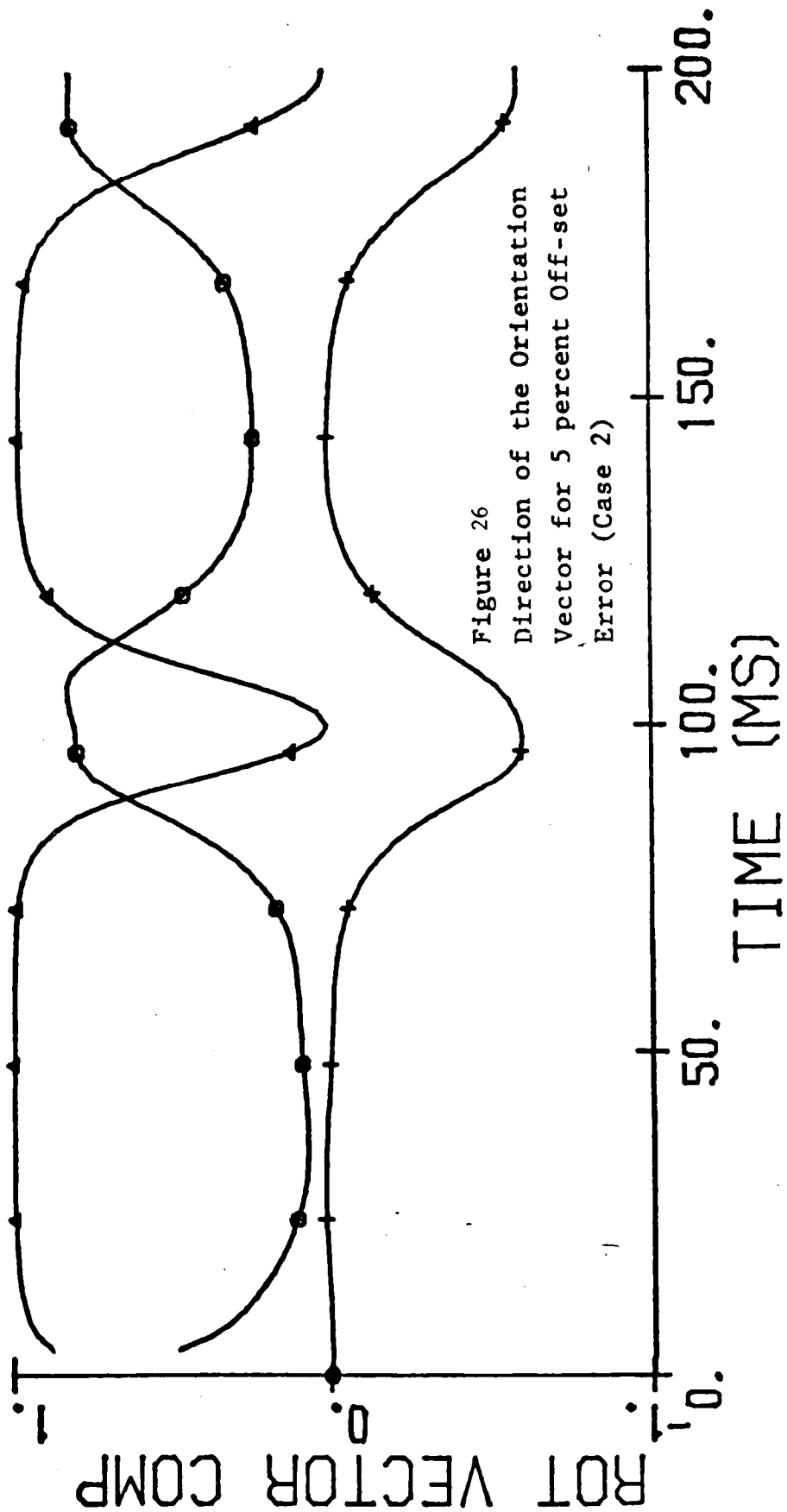
THETA

Figure 25
Orientation Vector Magnitude
for 5 percent off-set Error
(Case 2)



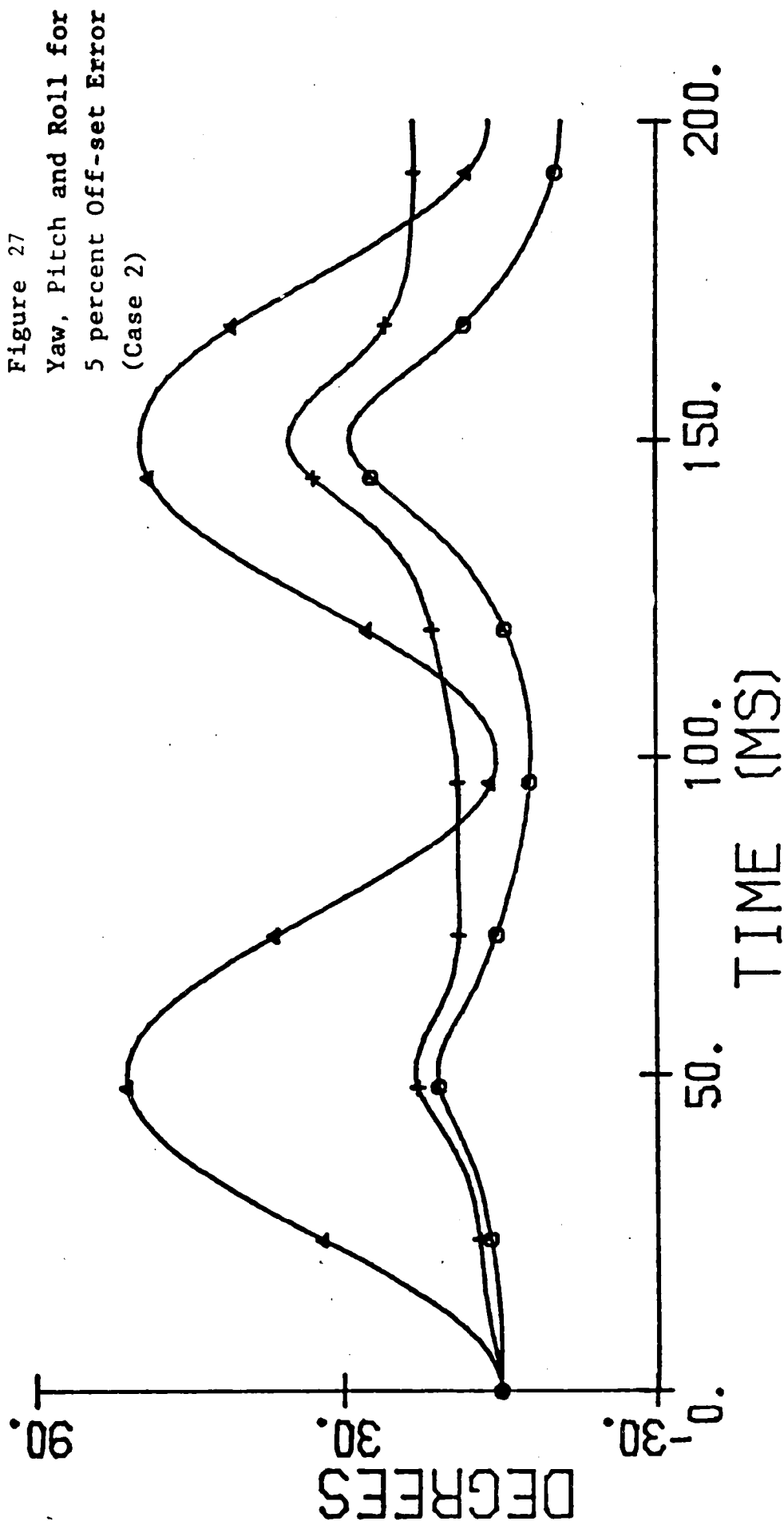
HYPH: CASE 2

TH-I
 TH-J
 TH-K



HYPH: CASE 2

○ YAW
 ▲ PITCH
 + ROLL



HYPH: CASE 2

S(TH/2) I
S(TH/2) J
S(TH/2) K
C(TH/2)

○
▲
+
x

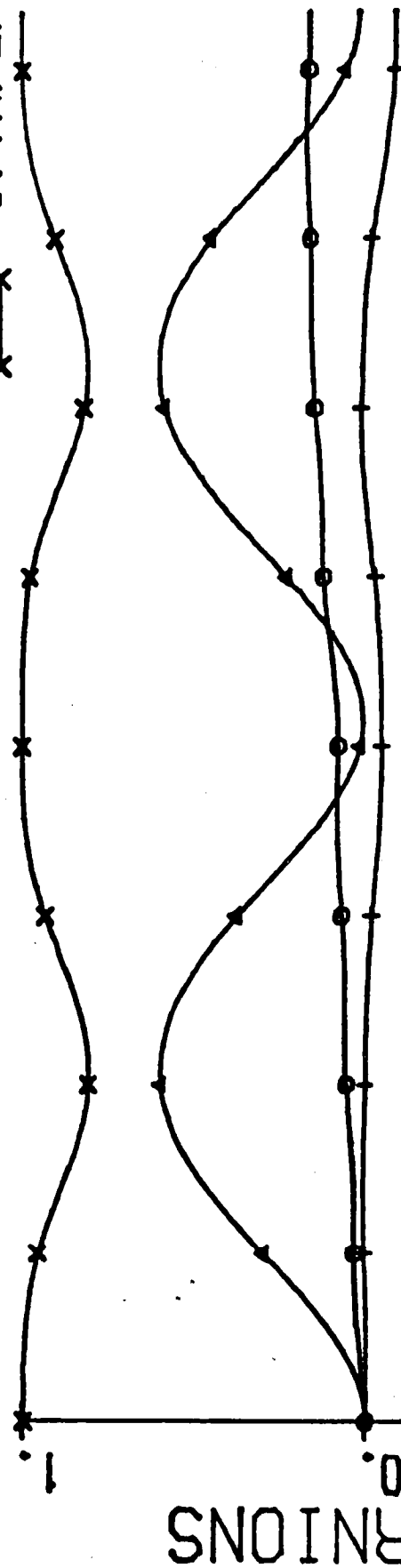
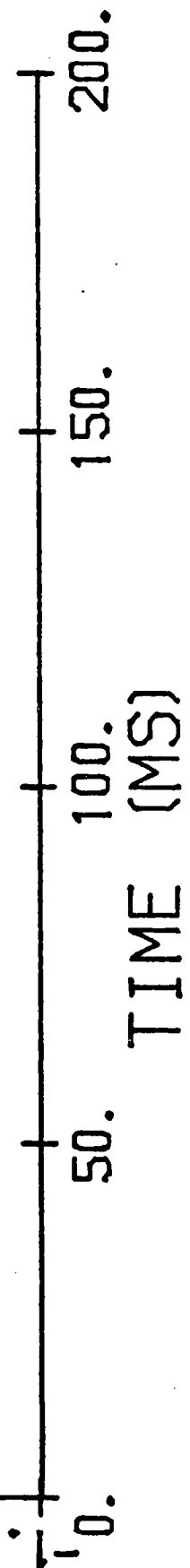


Figure 28
Quaternions for 5 percent
Off-set Error (Case 2)



HYPH: CASE 3

\bigcirc WX (B)
 \blacktriangle WY (B)
 $+$ WZ (B)

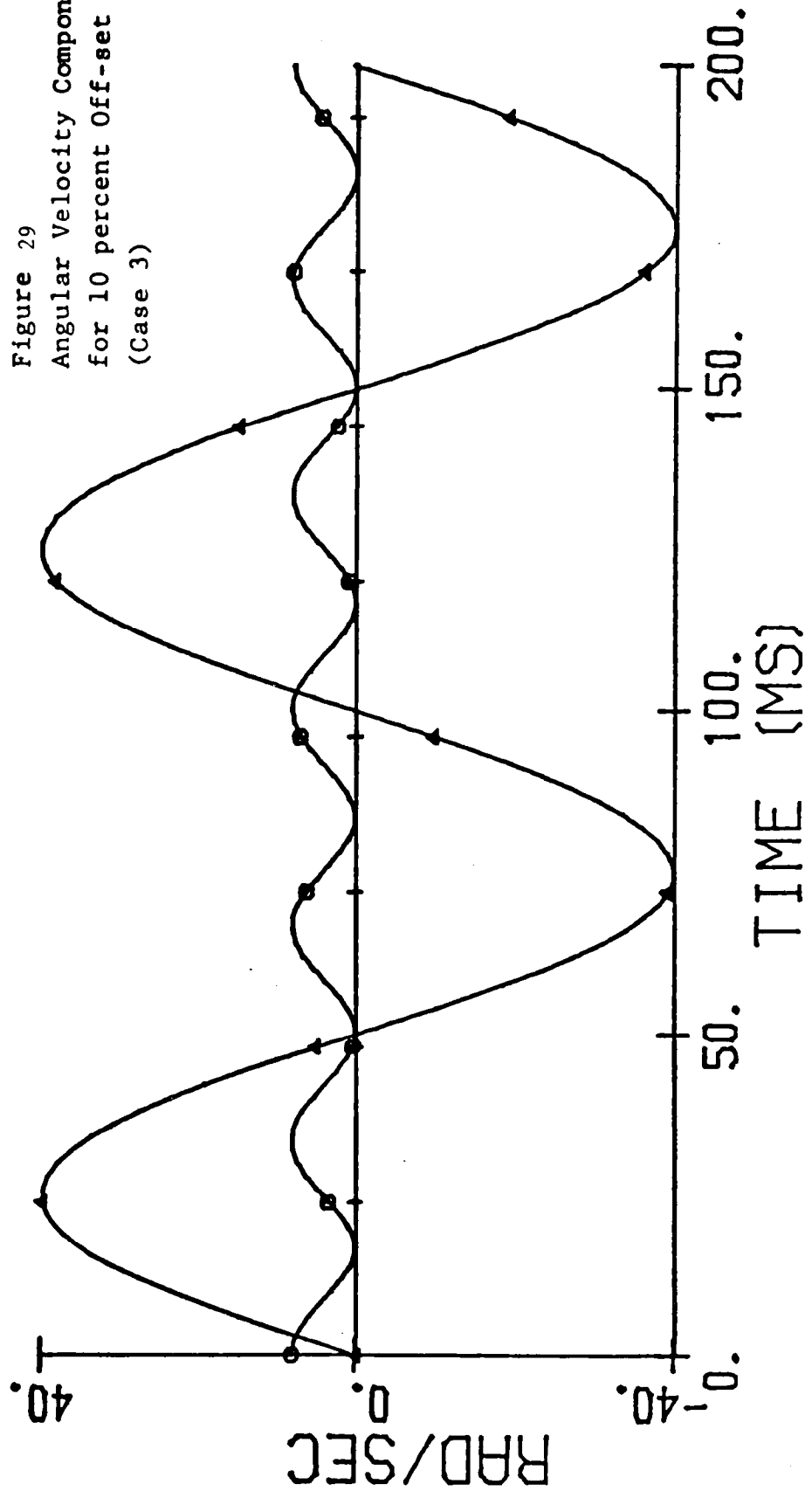


Figure 29
 Angular Velocity Components
 for 10 Percent Off-set Error
 (Case 3)

THETA

HYPTH: CASE 3

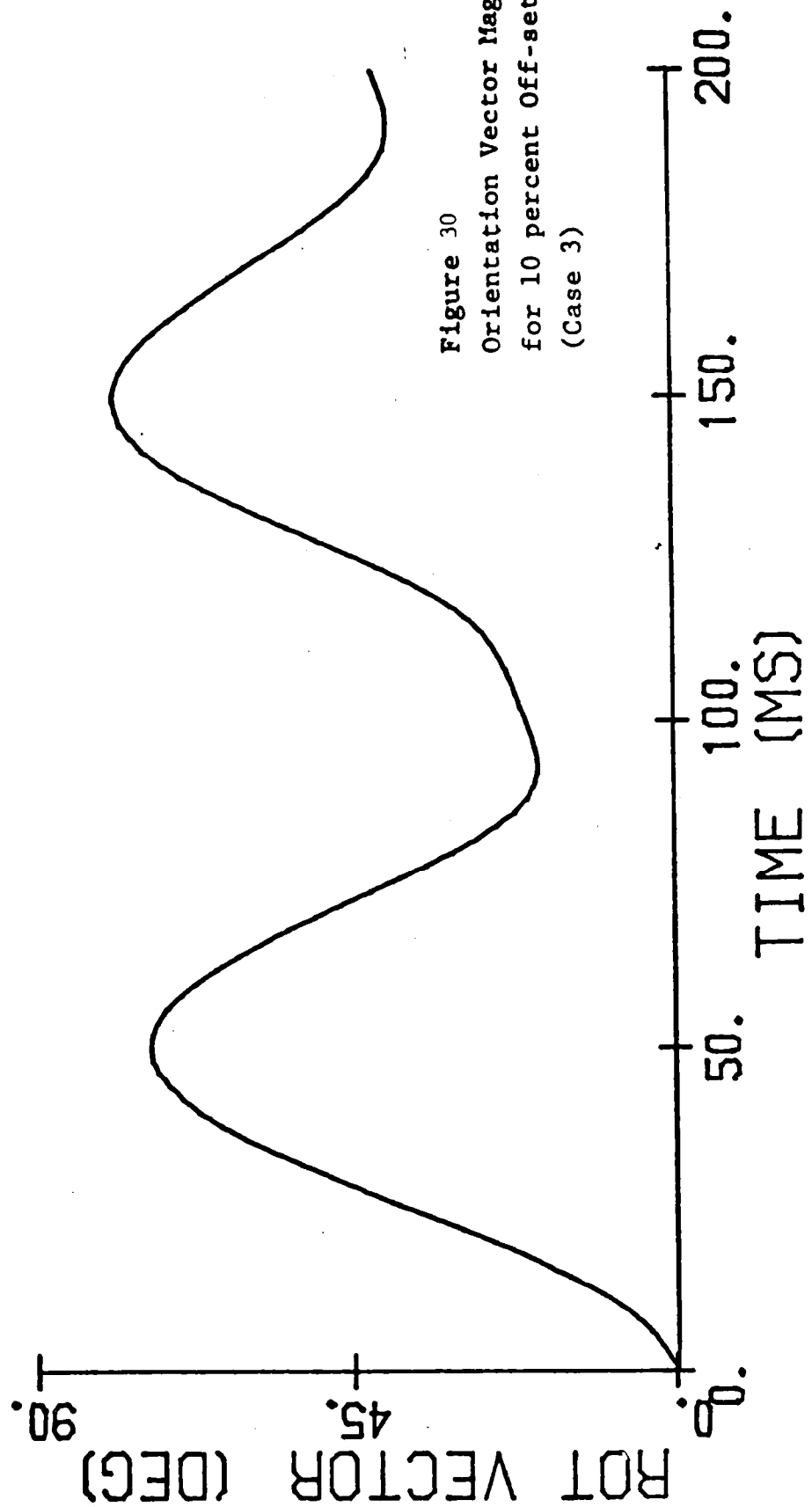
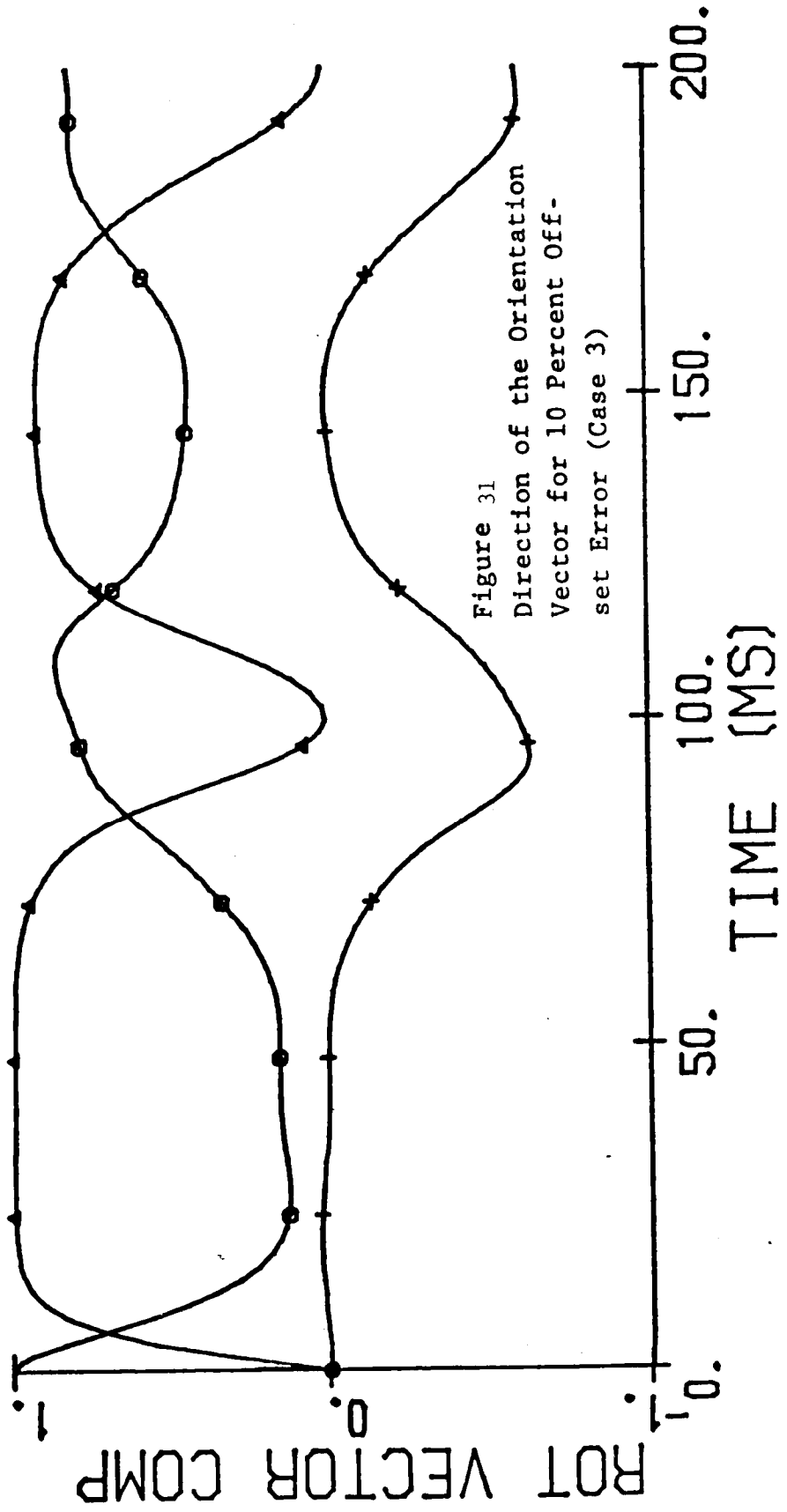


Figure 30
Orientation Vector Magnitude
for 10 percent Off-set Error
(Case 3)

HYPH: CASE 3

TH-I
TH-J
TH-K

○
△
+



HYPTH: CASE 3

YAW
PITCH
ROLL

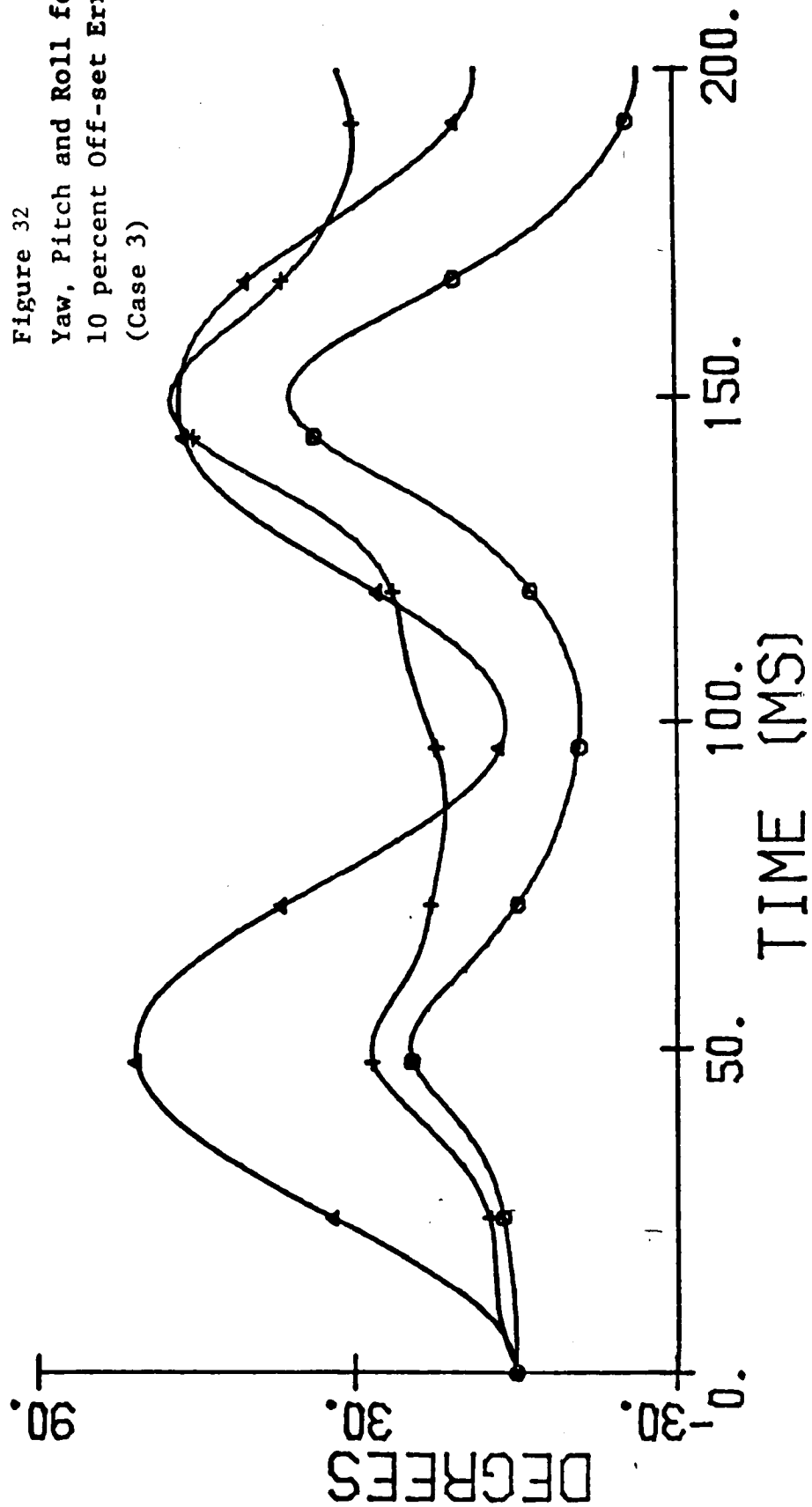


Figure 32

Yaw, Pitch and Roll for
10 percent Off-set Error
(Case 3)

HYPH: CASE 3

S(TH/2) I
S(TH/2) J
S(TH/2) K
C(TH/2)

○
△
+
x

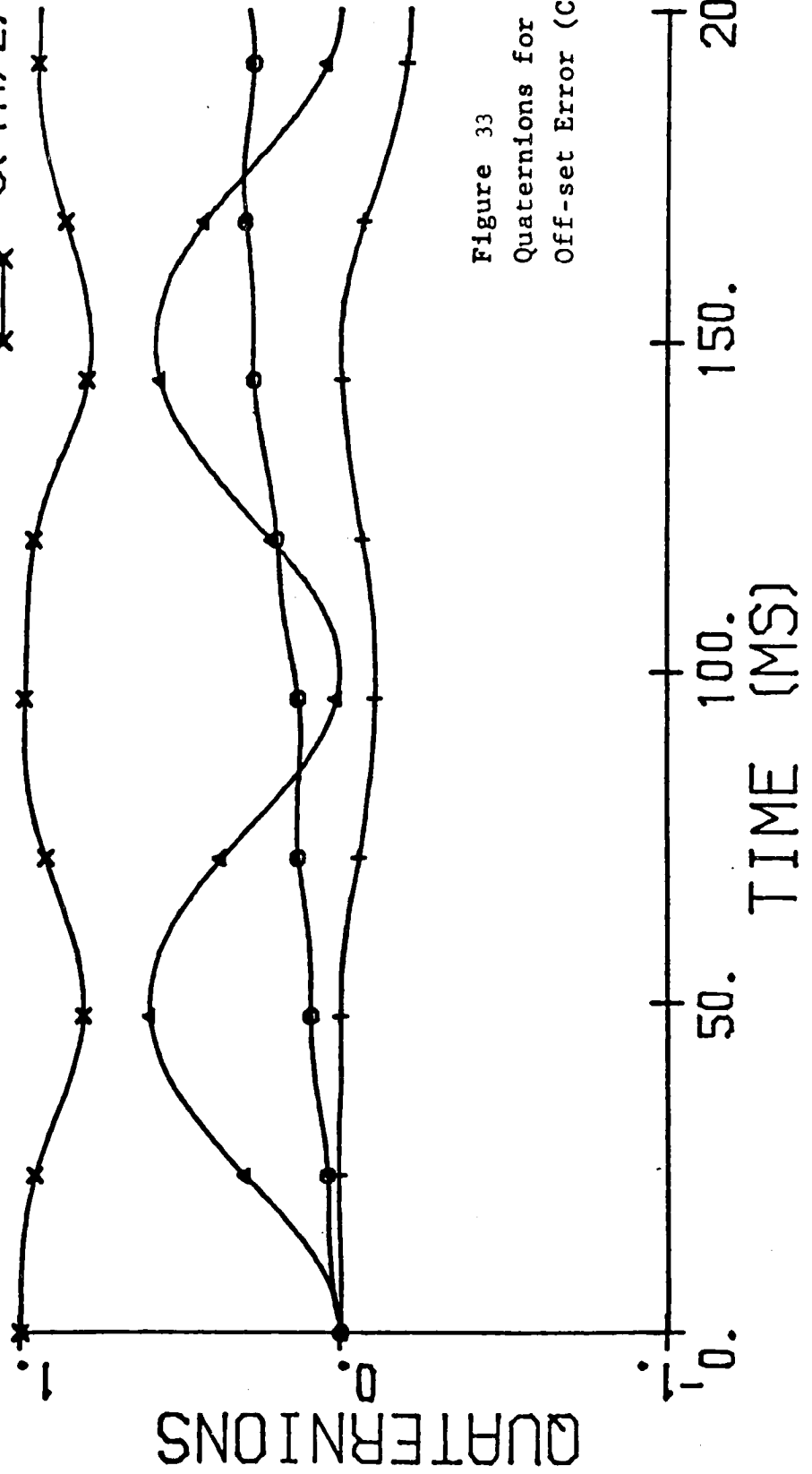


Figure 33
Quaternions for 10 percent
Off-set Error (Case 3)

